3

Enhancement of Wind Energy Penetration Levels using ADALINE-LMS Control Algorithm

This chapter presents an ADALINE-LMS controlled DSTATCOM based method for enhancing wind energy penetration level in the rural grid by mitigating the PQ disturbances under the MATLAB and experimental environments. Power quality issues associated with smooth grid synchronization, variable wind speeds, different grid strength, the various composition of loads and wind penetration levels have been investigated. Finally, the effectiveness of the proposed algorithm has been compared using algorithms published in the literature.

3.1 INTRODUCTION

Wind Energy (WE) sources are emerging as mainstream power specialists to reduce environmental pollution. Installation of WE sources can accommodate grid flexibility and minimize costs by adding technical advantages due to co-localization [Blaabjerg and Ma, 2017]. However, most of the WE sources are located far away from the strong grid, which leads to the weak grid integration of large wind turbines [Chen *et al.*, 2011]. High WE penetration into the weak grid presented multiple challenges to utilities due to unpredictable output, non-reliability, connected loads, interfacing converters, and the grid's strength [Saeedian *et al.*, 2020]. This is further aggravated in the presence of the non-linear (NL) loads connected at the Point of Common Coupling (PCC). Hence power quality such as harmonics, power factor (PF), reactive power, frequency and voltage stability have significantly deteriorated. Such deterioration in the quality of power majorly affects the soft synchronization [Wang *et al.*, 2020]. Therefore, the system is incapable of following IEEE-1547 international standard [C-2, 2018b]. However, accurate planning of reactive power and suitable PQ mitigation strategy with additional DSTATCOM infrastructure can solve the challenges as mentioned above, presented in [Zhou *et al.*, 2005].

3.2 CHOICE OF ADALINE-LMS CONTROL ALGORITHM OVER OTHER EXISTING CONTROL ALGORITHMS

Phase-Locked-Loop (PLL) technique makes the installed WE source's stable operation rely on a strong grid. But in the case of synchronization of DFIG in the weak grid, the power fluctuations that may increase the magnitude and frequency variations in the grid voltage can adversely affect the control performance of conventional PLL [Yuan *et al.*, 2010]. Because of these reasons, the side-band oscillations, small-signal and voltage stability issues are generated, and the current vector control scheme of the WE side converter does not provide the desired amount of reactive power [Zhang *et al.*, 2010]. [Durrant *et al.*, 2003], developed a low SCR model. The behaviour of this model demonstrates that weaker and unbalanced voltage in the system significantly affects the PLL's performance, which makes the Voltage Source Converter (VSC) more challenging to control. As a result, the maximum transmittable active power reduces. The inaccurate PLL gains deteriorate system stability [Hu *et al.*, 2014]. Thus, if the control parameters are not accurately calculated, it may lead to large fluctuations in the signals and not the right choice for smooth synchronization of

DFIG to a grid with high penetration levels.

Recently, the PLL-less idea for grid synchronization during high WE penetration has been prevalent to reduce the complexity and stability issues in the control algorithms. This idea directly utilized the DC-link voltage's intrinsic dynamics, which could maintain the large fluctuations in the frequency and voltage during the synchronization with low SCR of grids [Yang *et al.*, 2020; Khayat *et al.*, 2020]. [Huang *et al.*, 2017a] proposed a virtual synchronous controller for adopting grid impedance variations in the weak grid. The proposed controller effectively maintained the DC-link voltage dynamics to its reference value, keeping system frequency within the stability range (*i.e.* $\pm 10\%$). A synchronized control has been proposed in [Huang *et al.*, 2017b] for stability analysis in grid-tied WE source. Model-based [Elizondo *et al.*, 2014] and Model-free [Zhang *et al.*, 2020] predictive current controls have been developed for the soft grid synchronization of a DFIG in the strong grid. Abilash *et al.* [Thakallapelli *et al.*, 2019] presented the adaptive synchronized control for soft synchronization of DFIG into the strong grid. The outcomes of the research [Li *et al.*, 2019a] reveal that the soft synchronization of DFIG in a weak grid with high WE penetration can be possible with the proper reactive power planning and PQ mitigation through adaptive control techniques. Therefore, adaptive frequency estimation observer control has been developed for PQ mitigation in distorted grid conditions [Singh *et al.*, 2019]. However, the prominent feature wanted in the weak grid control and operation is the continuous and accurate tracking of the changes associated with system dynamics for meeting grid synchronization conditions.

In this context, adaptive filtering schemes were found suitable due to their salient feature of adopting changes with the system dynamics. Their parameters can be continuously updated for providing the desired output. [Haykin and Widrow, 2003], devised the LMS algorithm in 1959 in their research of pattern recognition machine, which is identified as the Adaptive Linear Neural-Network (ADALINE). This algorithm is broadly applied in several research areas, such as signal extraction, error minimization and noise reduction. [Singh *et al.*, 2007] *et al.*, utilized this concept for the power quality mitigation. They considered the idea for calculating weights of the fundamental active component and the reactive component of load current based on the least mean square filter and further its training with adaptive linear neural network structure for harmonics mitigation in a utility network. However, the proposed ADALINE-LMS adaptive control algorithm ensures reliable operation with maintaining PQ standards due to the attractive features, including simple architecture, simplified calculation, Experimental compatibility, PLL-less structure, adaptiveness, minor steady-state error, and accuracy of estimation of power.

3.3 SYSTEM CONFIGURATION

The system configuration of the rural grid with high WE penetration is depicted in Fig. 3.1, where the DSTATCOM is employed to inject the reactive power and improve the PQ for enhancement of WE penetration into the rural grid. The base MVA and base voltage are selected to be 4.5 MW and 0.415 kV, respectively, for the per-unit (p.u.) calculations. The details of the various parameter used for the system configuration is presented in Table 3.1.

3.4 DESIGNING OF ADALINE-LMS ALGORITHM

The design considerations of the basic and proposed ALMF algorithm is explained in following subsections.

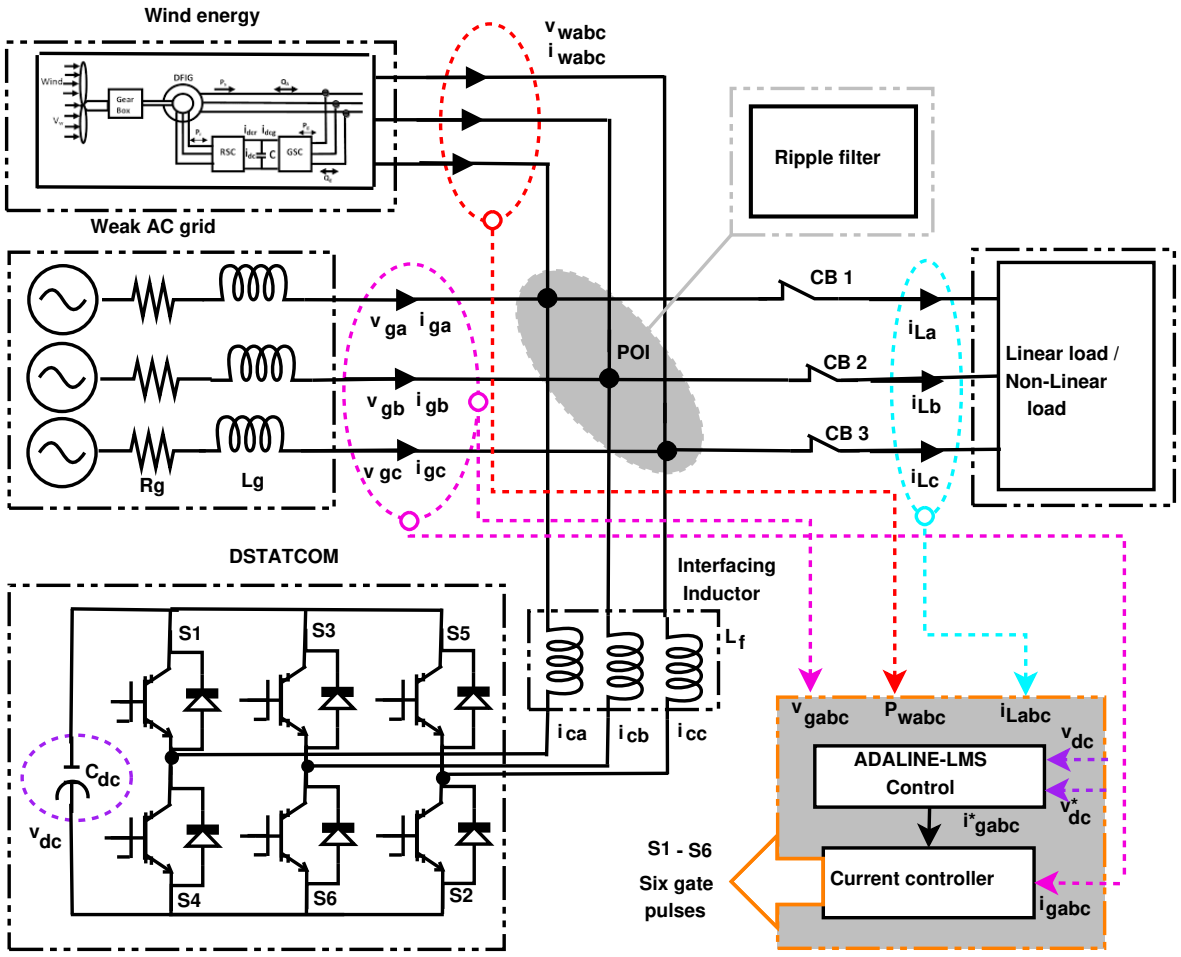

Figure 3.1: The system configuration of the rural grid.

Table 3.1: System parameters.

Parameters	MATALB simulation values	Experimental values
Type-III DFIG	1.5 MW,3 MW,4.5 MW,6 MW	0.400 kW
WE penetration level (25%)	4.5 MW, 575 V	0.400 kW, 415 V
Wind speed variations	15 m/s and 7.5 m/s	12 m/s and 7.2 m/s
SCR of grid	2.74, 5 and 7	2.74, 5 and 7
X/R ratio of grid	7	7
Step down transformer	575 V / 415 V	-
Linear loads at 0.8-lagging PF (100%)	18 MW	1.6 kW
Linear loads at 0.8-lagging PF (75%)	13.5 MW	1.2 kW
Rectifier based NL loads (25%)	4.5 MW	0.4 kW
DSTATCOM	4.5 MVAr, 680 Vdcd	5 kVAr, 500 Vdcd

3.4.1 Standard LMS Algorithm

The Least Mean Square (LMS) adaptive algorithm aims to identify the unknown coefficients vector adaptively by using the input signal $X(n)$ and the output $Y(n)$. The unknown system is shown in Fig. 3.2. In this system, the coefficients vector (W) of an N-length finite impulse response

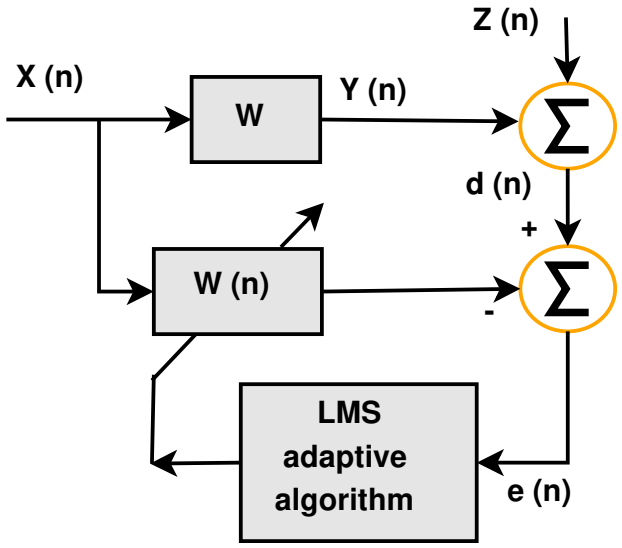

Figure 3.2: Weight updation of standard adaptive LMS algorithm.

(FIR) filter and input signal vectors are defined as $W = [w_1, w_2, ..., w_N]^T$ and $X(n)$=$[x(n), x(n-1), ..., x(n-(N+1))]^T$, respectively. However, noise is represented by $Z(n)$, which is assumed to be independent with $X(n)$.

$$Y(n) = W^T \times X(n) + Z(n) \tag{3.1}$$

Let, $W(n)$ be the estimated coefficients-vector at n^{th} iteration, then instantaneous estimation error is express as $e(n) = Y(n)W^T(n) \times X(n)$ [Gui *et al.*, 2014]. The cost function $L_{lms}(n)$ of standard LMS algorithm is written as,

$$L_{lms}(n) = 1/2(e^2(n)) \tag{3.2}$$

The algorithm coefficients-vector $W(n)$ is updated using LMS equation,

$$W(n+1) = W(n) - \mu(\partial L_{lms}(n)/\partial W(n)) \tag{3.3}$$

$$W(n+1) = W(n) + \mu \times e(n) \times X(n) \tag{3.4}$$

The range described in [Singh *et al.*, 2007] for μ is 0.01 to 1.0. The selection of μ increases the accuracy and the rate of convergence. Higher the value of μ, the convergence rate increases, but the accuracy is decreased. The low value of μ gives good accuracy, but the rate of convergence is slow [Haykin, 2008].

3.4.2 Proposed ADALINE-LMS Control Algorithm

The ADALINE-LMS control algorithm estimates the active and reactive weight components of load currents taking care of changes in wind generation, load current, DC-link voltage and grid voltage. These weights are used to generate reference current signals to switch the DSTATCOM. The AC grid voltage is written as,

$$v_g = v_1 sin(wt) + \sum_{n=2}^{\infty} v_n sin(nwt + \phi_n) \tag{3.5}$$

Grid voltage and phase angle are v_g and ϕ, respectively. The unit voltage templates for a single-phase is written as,

$$v_p(t) = V sin(nwt) = u_{pa} \tag{3.6}$$

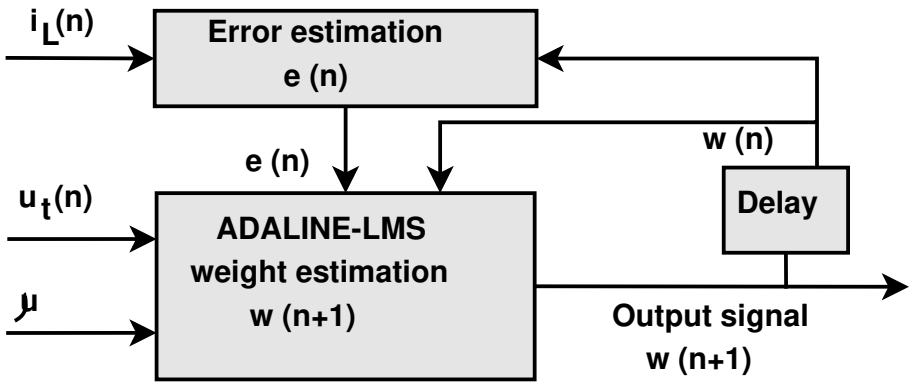

Figure 3.3: Block diagram of weight estimation using the ADALINE-LMS algorithm.

$$v_q(t) = Vcos(nwt) = u_{qa} \tag{3.7}$$

The load current is express as,

$$i_L(t) = I_1 sin(wt + \phi_1) + \Sigma I_n sin(nwt + \phi_n) \tag{3.8}$$

Equation (3.8) can also be written as,

$$i_L(t) = i_1(t) + i_h(t) = i_{1p}(t) + i_{1q}(t) + i_h(t) \tag{3.9}$$

where, $i_h(t)$ is the harmonic current component. However, the active current $i_{1p}(t)$ component and reactive current $i_{1q}(t)$ components are helps to estimate the fundamental current signal $i_1(t)$. The calculation of active and reactive components are written as,

$$i_{1p}(t) = W_p \times u_p, i_{1q}(t) = W_q \times u_q \tag{3.10}$$

Harmonic components of load current can be express as,

$$i_h(t) = i_L(t) - i_{1p}(t) - i_{1q}(t) \tag{3.11}$$

The proposed algorithm is designed in such a way that the system signals continuously update ($w(n+1)$) weight components in order to mitigate harmonics (i_h) in the system. The block diagram of weight estimation using the ADALINE-LMS algorithm is as presented in Fig. 3.3. It can be observed that weights are estimated and updated after every iteration. The error signal ($e(n)$) is calculated using load current ($i_L(n)$), weight component ($w(n)$), and grid voltage unit templates ($u_t(n)$). The detailed ADALINE-LMS algorithm is shown in Fig. 3.4.

1. **Estimation of Active Power Component of Reference Grid Current Signals:** The peak amplitude of ac terminal voltage (v_t) at PCC is determined from 3-phase weak grid voltages.

$$v_t = \sqrt{2/3(v_{ga}^2 + v_{gb}^2 + v_{gc}^2)} \tag{3.12}$$

Sensed three-phase grid voltages are divided by the terminal voltage to obtain active unit templates. Initially, these templates are not unity due to the low SCR of the grid. The primary condition of grid synchronization requires the matching of amplitude and phase of the ac grid voltage with the amplitude and phase of WE voltage in respective order. Therefore, to meet these conditions active unit voltage template plays an important role when it is maintained at unity [Mohod and Aware, 2010]. Estimation of unit voltage templates are as follows,

$$u_{pa} = \ v_{ga}/v_t; u_{pb} = \ v_{gb}/v_t; u_{pc} = \ v_{gc}/v_t \tag{3.13}$$

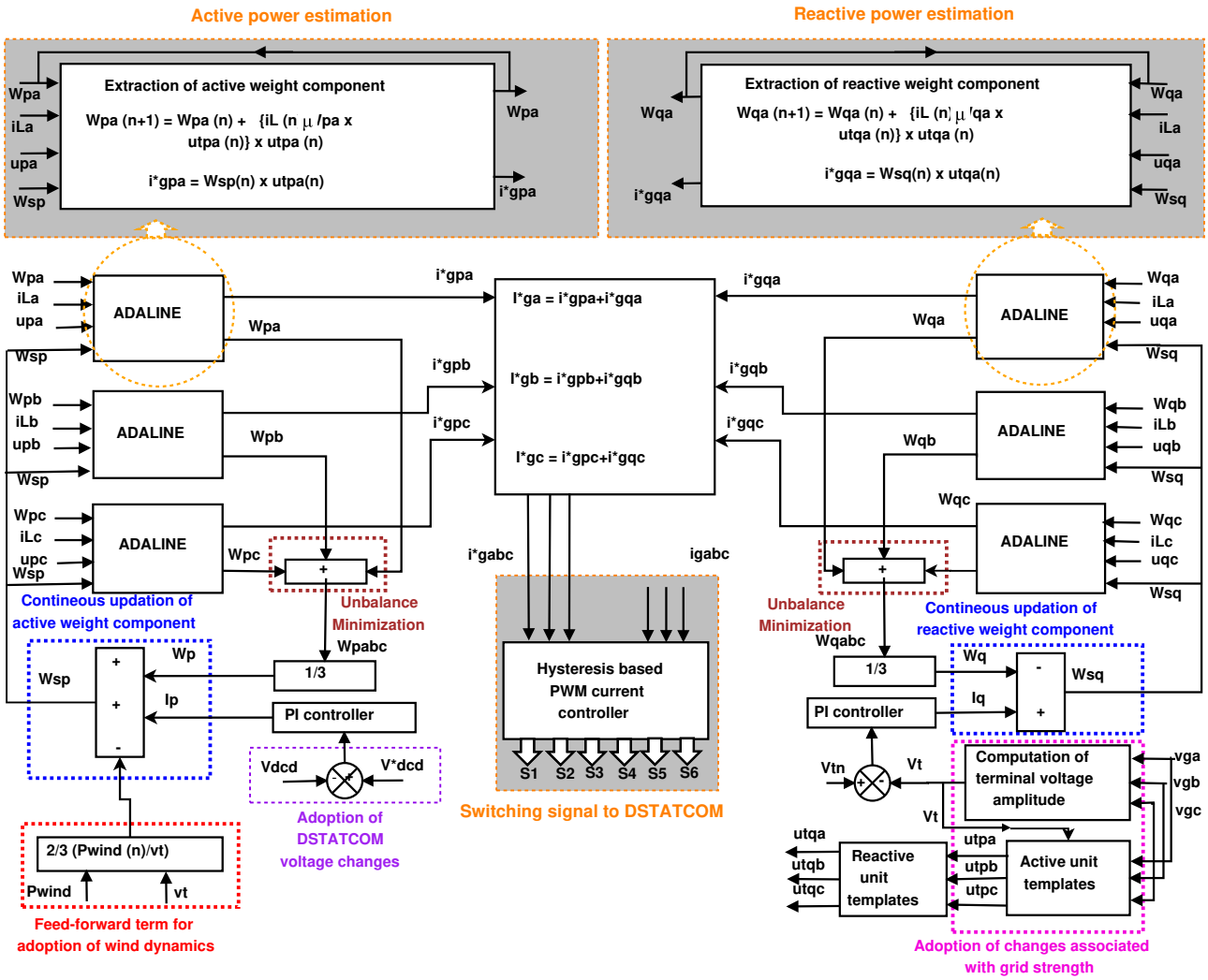

Figure 3.4: Block diagram of proposed ADALINE-LMS control algorithm.

The accurate estimation of DC link voltage is essential because if it is maintained to its reference voltage then the frequency fluctuations and voltage fluctuations can be minimized significantly during the synchronization. In this regard, the PI regulator has tuned with the optimum value of proportional $K_{pd} = 0.3$ and integral $K_{id} = 0.001$ gains. This voltage regulator generates an active loss component $I_p(n)$ for maintaining dc-bus voltage at n^{th} sampling instant,

$$I_p(n) = W_{sp}(n-1) + K_{pd}v_{de}(n) - v_{de}(n-1) + K_{id}v_{de}(n) \tag{3.14}$$

$W_{sp}(n-1)$: preceding active loss component, $v_{de}(n-1)$: DC voltage error. However, the current value of voltage error (v_{de}) is computed using the reference DC bus voltage of DSTATCOM (v^*_{dcd}).

$$v_{de}(n) = v^*_{dcd}(n) - v_{dcd}(n) \tag{3.15}$$

However, the reference DC bus voltage of DSTATCOM is calculated as,

$$v^*_{dcd} = 2\sqrt{2}v_{LL}/\sqrt{3}m \tag{3.16}$$

v_{LL} represents voltage (line to line) at PCC, and m is the modulation index.

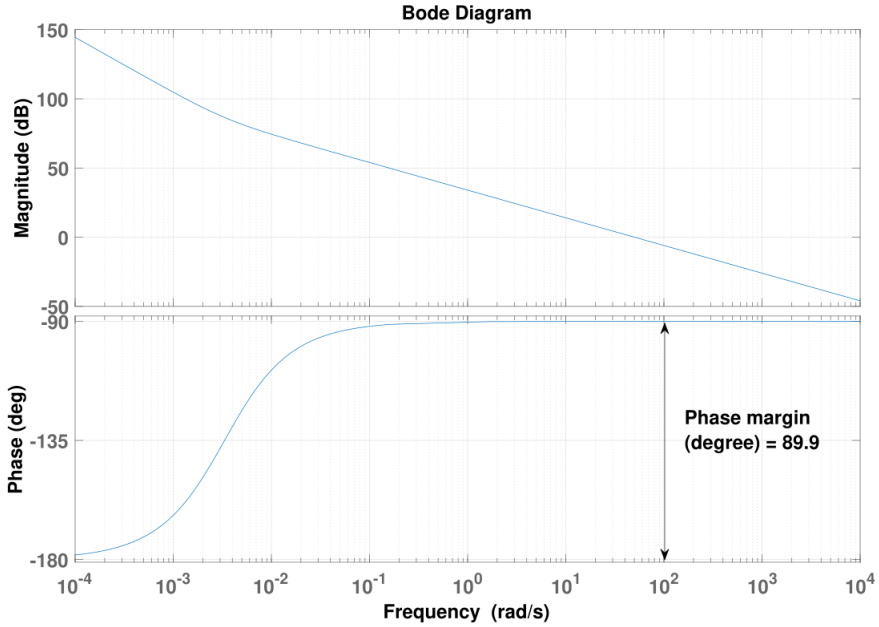

Figure 3.5: Bode stability diagram of ADALINE-LMS control using controller inputs.

The stability investigation of the system is carried out for DSTATCOM dc-link control using the Bode stability plot. The transfer function ($G_S(s)$) of the system is estimated as [Agarwal *et al.*, 2017a]:

$$G_s(s) = G_p(s) \times G_c(s) = [(1/sc_{dc}) \times (k_p + k_i/s)] \tag{3.17}$$

where, G_p(s) and G_c(s) are the plant and PI voltage regulator transfer functions. The Bode stability diagram is plotted for G_s(s) with the help of system parameters as depicted in Fig 3.5. The Bode stability plot illustrates that the system is stable because phase margin is found in the stable region.

Wind-feed-forward term (W_{wind}) is implemented in the algorithm to adapt the changes in the current output power (P_{wind}) of WE source. It can be calculated as,

$$W_{wind}(n) = 2P_{wind}(n)/3v_t \tag{3.18}$$

However, to minimize the effect of load current during synchronization weights are averaged. The fundamental active weight component of reference grid currents is,

$$W_p(n) = \{W_{pa}(n) + W_{pb}(n) + W_{pc}(n)\}/3 \tag{3.19}$$

Where, $W_{pa}(n)$, $W_{pb}(n)$ and $W_{pc}(n)$ are weight components of load current signals corresponding to all phases. For the accurate adoption of system dynamics in the algorithm, the total weight component should update with the changes associated with the DSTATCOM. Thus, output of PI regulator $I_p(n)$ should be added to the averaged weight component $W_p(n)$ and subtract with the feed-forward wind weight component ($W_{wind}(n)$) to form updated total weight component $W_{sp}(n)$.

$$W_{sp}(n) = W_p(n) + I_p(n) - W_{wind}(n) \tag{3.20}$$

The active weight components of 3-phase load currents are extracted using an individual ADALINE in each phase.

$$W_{pabc}(n+1) = W_{pabc}(n) + \mu\{i_{Labc}(n) - W_{pabc}(n)u_{pabc}(n)\}u_{pabc}(n) \tag{3.21}$$

Where, $W_{pabc}(n+1)$ are updated active phase-a,b and c weight components of load current, μ is step size, i_{Labc} are load currents and u_{pabc} are active weak grid voltage unit templates. Accuracy of estimation and convergence are based on the value of convergence factor (μ) and it is selected as 0.02.

The reference active components of weak grid currents are,

$$i^*_{gpabc} = W_{sp} \times u_{pabc} \tag{3.22}$$

2. **Estimation of Reactive Power Component of Reference Grid Current Signals:** The quadrature unit templates of three-phase weak grid voltage are derived using active unit templates as,

$$\left\{\begin{array}{c} u_{qa} = -u_{pb}/\sqrt{3} + u_{pc}/\sqrt{3} \\ u_{qb} = \sqrt{3}u_{pa}/2 + (u_{pb} - u_{pc})/2\sqrt{3} \\ u_{qc} = -\sqrt{3}u_{pa}/2 + (u_{pb} - u_{pc})/2\sqrt{3} \end{array}\right\} \tag{3.23}$$

The PI voltage regulator maintain terminal voltage at PCC by generating reactive loss component $I_q(n)$. This loss component is used to regulate AC voltage at n^{th} sampling instant,

$$I_q(n) = W_{sq}(n-1) + K_{pq}v_{te}(n) - v_{te}(n-1) + K_{iq}v_{te}(n) \tag{3.24}$$

K_{pq} and K_{iq} are reactive PI gains of Proportional Integral regulator. Also, $W_{sq}(n-1)$ denoted by preceding reactive loss component and $v_{te}(n-1)$ ac voltage error. However, the present value of this voltage error (v_{te}) is,

$$v_{te}(n) = v_{tn}(n) - v_t(n) \tag{3.25}$$

The weights of the fundamental q-axis (reactive component) component of reference grid currents is given as,

$$W_q(n) = \{W_{qa}(n) + W_{qb}(n) + W_{qc}(n)\}/3 \tag{3.26}$$

Where, $W_{qa}(n)$, $W_{qb}(n)$ and $W_{qc}(n)$ are weight components of load current signals. However, averaging the weights helps to minimize the effect of the load current component during synchronization. For the accurate adoption of system dynamics in the algorithm, the total weight component should update with the changes associated with the DSTATCOM. Thus, the output of PI regulator $I_q(n)$ should be subtract to the averaged weight component $W_q(n)$ to form updated total weight component $W_{sq}(n)$.

$$W_{sq}(n) = W_q(n) - I_q(n) \tag{3.27}$$

The reactive weight components of 3-phase load currents are extracted using an individual ADALINE in each phase.

$$W_{qabc}(n+1) = W_{qabc}(n) + \mu\{i_{Labc}(n) - W_{qabc}(n)u_{qabc}(n)\}u_{qabc}(n) \tag{3.28}$$

Where, $W_{qabc}(n+1)$ are updated phase-a, b and c reactive weight component of load current, μ is step size. The reference components of grid currents are,

$$i^*_{gqabc} = W_{sq} \times u_{qabc} \tag{3.29}$$

Thus, three-phase reference weak grid currents are generated by adding active and reactive reference signal (i^*_{gpa}), (i^*_{gpb}), (i^*_{gpc}) and (i^*_{qa}),(i^*_{qb}), (i^*_{qc}) respectively.

$$i^*_{gabc} = i^*_{gpabc} + i^*_{gqabc} \tag{3.30}$$

3. **Generation of Switching Signals** The hysteresis current controller (HCC) is utilized to generate six-gating signals for DSTATCOM switches, where 3-phase estimated grid signals (i^*_{gabc}) are compared with the sensed weak grid signal (i_{gabc}). In this context two logics are employed, If (i_{gabc}) > ($i^*_{gabc} + hcb$), the lower switch is OFF and the upper switch is ON. If (i_{gabc}) < ($i^*_{gabc} - hcb$), the upper switch is OFF and the lower switch is ON.

3.5 SIMULATION RESULTS AND DISCUSSIONS

The performance of the proposed methodology has been demonstrated by simulating unbalance with various strengths of the grid, different compositions of the loads and various penetration levels of WE. The description of the case studies is presented in Table 3.2.

Table 3.2: Parameter variations for various case studies.

S.No.	Parameters	Parameter Variations	
		Simulation	Experimental
1	SCR	2.74, 5 and 7	2.74, 5 and 7
2	Load-1	100% linear 0.8 lag-PF load	100% linear 0.8 lag-PF load
3	Load-2	25% NL load + 75% linear load	25% NL load + 75% linear load
4	WE Penetration levels	10%, 18%, 25% and 30%	10%, 18%, 25% and 30%
5	Wind speed variation	15 m/s - 7.5 m/s	12 m/s - 7.2 m/s
6	Synchronization point	at 1 second	at 1 second

3.5.1 Case-1: Enhancement of WE Penetration Levels

Figure 3.6 presents the penetration levels of wind energy sources. The penetration levels are enhanced from 10% to 30% into the grid of SCR 2.74 with 100% linear load. It can be found that the power quality of the system in terms of voltage is maintained within the stability range

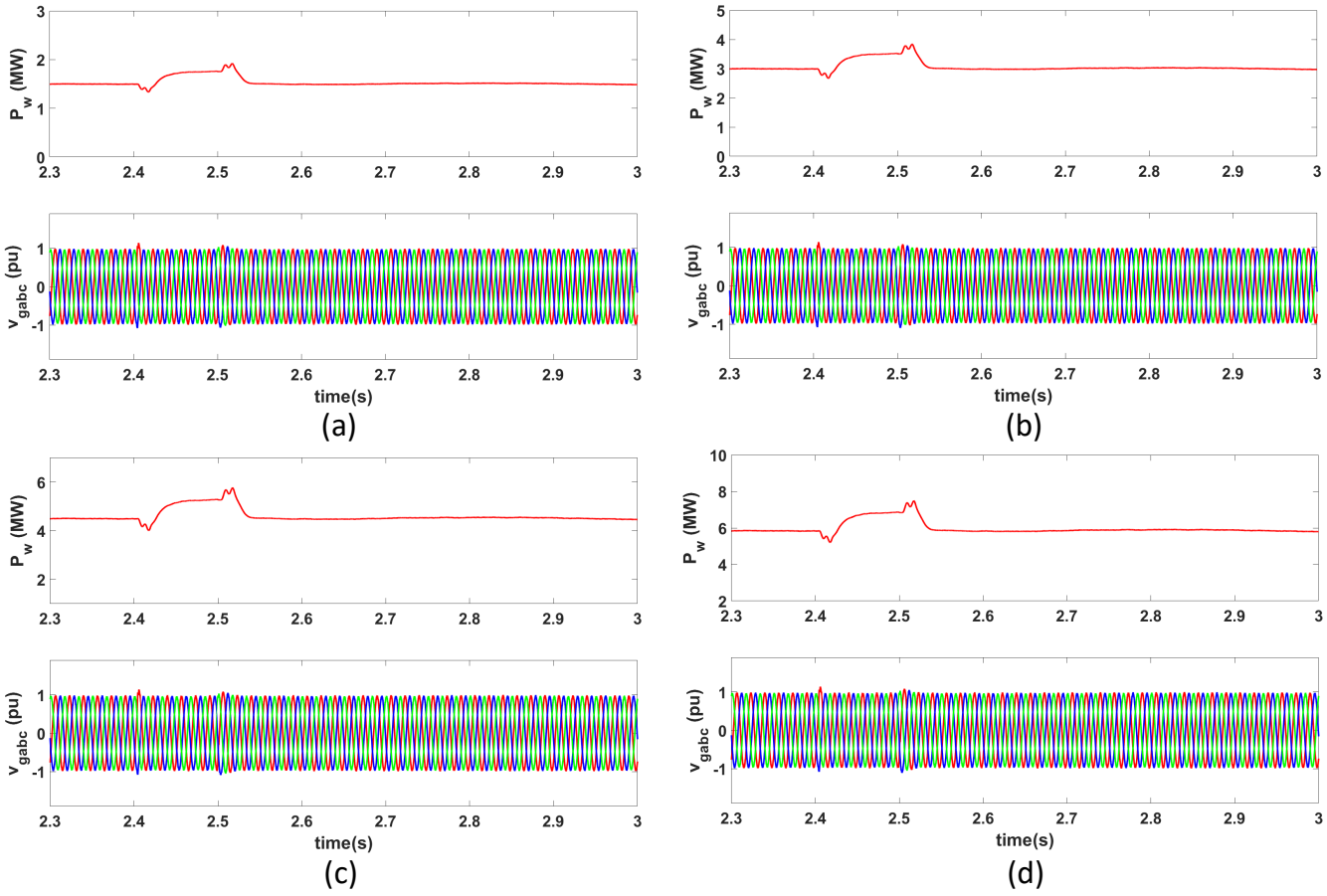

Figure 3.6: WE penetration levels with 100% linear load (a) 10%, (b) 18%, (c) 25%, (d) 30%.

Table 3.3: Enhancement of WE penetration levels (Simulation).

Penetration	Loads (→)	Load-1		
levels (↓)	SCR (→)	2.74	5	7
Simulation analysis				
10%	V_{gTHD}	2.175	2.151	2.140
	i_{gTHD}	0.627	0.603	0.592
	PF_g	1	1	1
	P_w (MW)	1.5	1.5	1.5
	Q_d (MVAr)	0.410	0.401	0.392
	V_g (Volt)	418	417	416
18%	V_{gTHD}	2.289	2.251	2.230
	i_{gTHD}	0.685	0.661	0.620
	PF_g	1	1	1
	P_w (MW)	3	3	3
	Q_d (MVAr)	0.495	0.481	0.473
	V_g (Volt)	419.09	418.02	416
25%	V_{gTHD}	2.55	2.50	2.47
	i_{gTHD}	0.71	0.70	0.68
	PF_g	0.99	0.99	0.99
	P_w (MW)	4.5	4.5	4.5
	Q_d (MVAr)	0.99	0.945	0.9
	V_g (Volt)	428.37	428.02	426
30%	V_{gTHD}	4.34	4.22	4.27
	i_{gTHD}	1.88	1.80	1.77
	PF_g	0.89	0.89	0.89
	P_w (MW)	5.56	5.56	5.56
	Q_d (MVAr)	1.96	1.87	1.78
	V_g (Volt)	420.2	420.01	419.7

($i.e. \pm 10\%$) up to 30% WE penetration level. However, up to 25%, the active power of WE sources is tracked with more than 99% accuracy, and beyond 25%, the wind power tracking deteriorated due to PQ issues. The simulation results are shown in Table 3.3. It is found that increments in the penetration level up to 30% harmonic levels also increase in the system. These harmonic levels are well maintained under the international PQ standards. The power factor, the magnitude of voltage and harmonic levels of voltage and current of the grid are observed to meet PQ standards with increments in the penetration level. It has also been observed that the presence of non-linear load also deteriorates the PQ and limit the wind energy penetration levels.

3.5.2 Case-2: Performance with NL Load at Rated Wind Speed

Figure 3.7 presents the various waveforms associated with the case study for mitigating the PQ of the grid with an SCR of 2.74. This case study considers a load combination of 25% Nonlinear + 75% linear loads and 25% WE penetration. An unbalance simulated from 2.4-second to 2.5-second by disconnecting phase-a of load and connecting it back. The interval 2.48-second - 2.535-second illustrate recovery stage, as shown in Fig. 3.7 (a). During the unbalancing, the DSTATCOM continuously supplies compensating current (i_{cabc}) to maintain grid voltage (v_{gabc}) and to compensate the unbalance in the grid current. The total recovery time from the unbalance stage to the balance stage is found to be 0.04-second, which illustrates the fast adaptive capability of the proposed control. The DC-link voltage of the DSTATCOM (v_{dcd}) is maintained at its reference

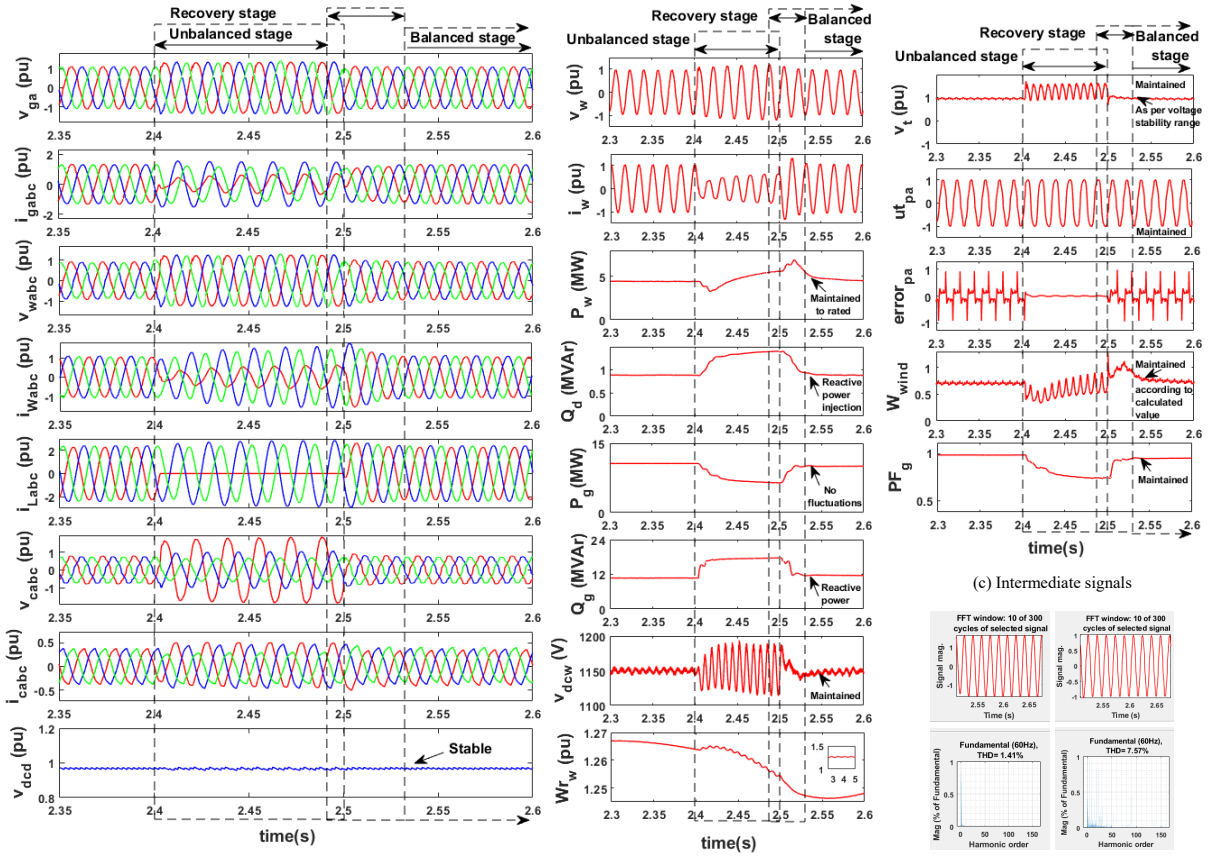

(a) System waveforms (b) Grid and Wind signals (c) Intermediate signals (d) Grid current and voltage harmonics

Figure 3.7: Performance of proposed method with NL load at rated wind speed.

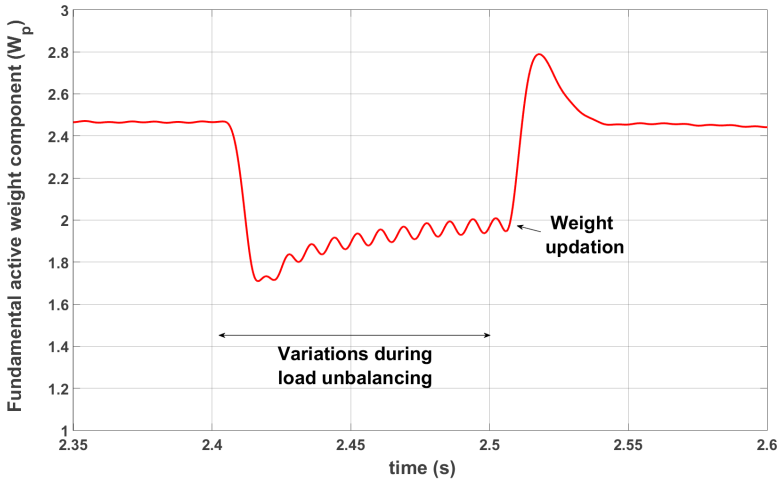

Figure 3.8: Updation of weight component of load current.

value. Fig. 3.7 (b) illustrates the performance of DSTATCOM to maintain the rated active-power injection from the WE ($P_w = 4.5$ MW). It also evident that the increased reactive-power demand by the grid (Q_g) during load unbalancing is effectively compensated by the proposed method. The DC-link voltage (V_{dcw}) of the wind side converter is maintained at 1150 V. The rotor oscillations of wind generator (Wr_w) are found to be practically damped.

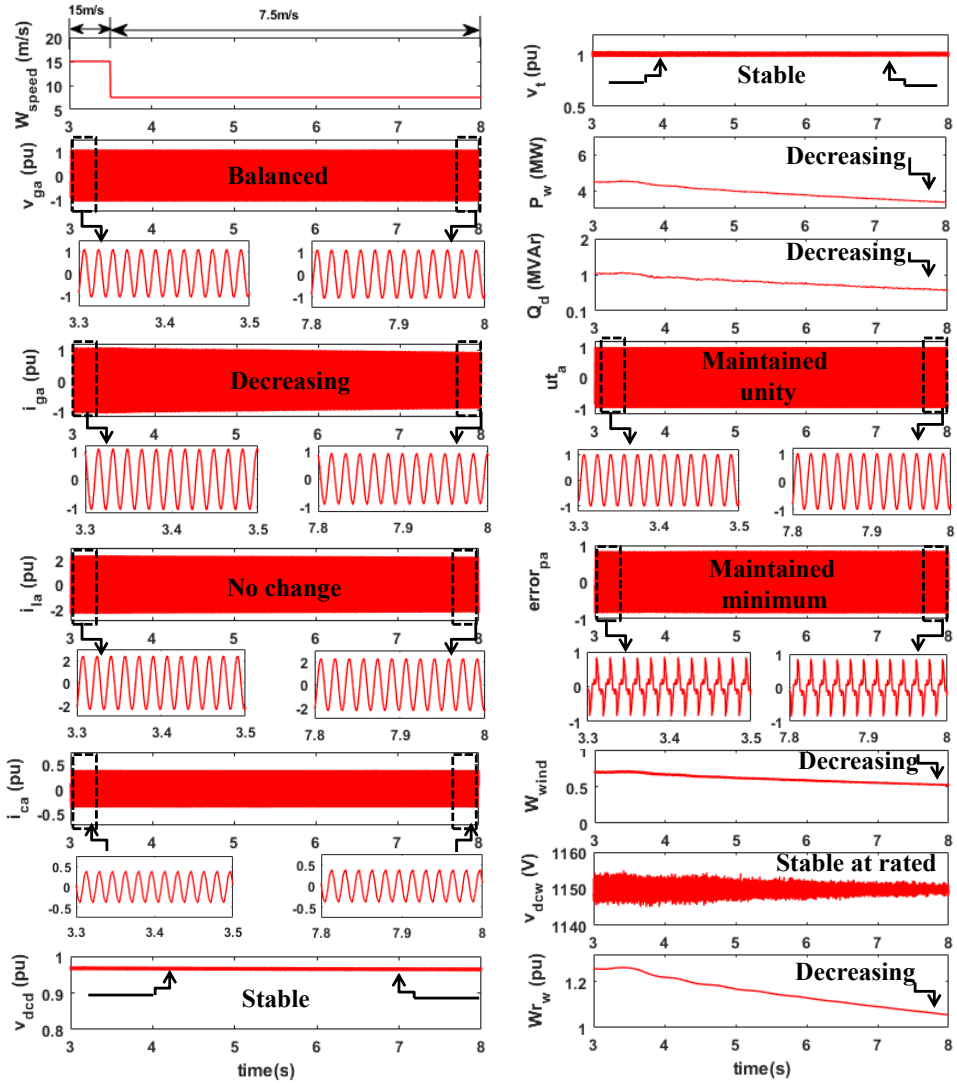

(a) System waveforms

(b) Intermediate signals

Figure 3.9: Performance of proposed method with NL load at minimum wind speed.

The size of DSTATCOM has been considered 4.5 MVAr, without a controller. However, after implementing the proposed adaptive control algorithm, the optimized reactive power injected by DSTATCOM during 25% WE penetration is approximately 1.2 MVAr. This result shows the size of DSTATCOM is reduced by 70% due to effective control actions of the adaptive control algorithm.

The waveforms of intermediate signals are computed in the ADALINE-LMS control algorithm depicted in Fig. 3.7 (c). It can seen from the Fig. 3.7 (c) that, At 2.4-second DSTATCOM provides rapid compensating current (i_{cabc}) to stabilize the terminal voltage (V_t) by keeping grid unit templates (ut_{pa}) at unity. The current error ($error_{pa}$) is found to be minimum. The calculated and simulated results of the wind feed-forward term are found to be the same ($\sim$ 0.66 A). Fig. 3.7 (d) shows the grid current harmonics (0.71%) and voltage harmonics (7.57%), which lies within the unit of PQ standards. The weight component of load currents (W_{pa}) is shown in Fig. 3.8 It can be observed that the oscillations in the signal are significantly less even during the load unbalancing. The weight component is continuously updated with good accuracy of tracking.

3.5.3 Case-3: Performance with NL Load at Minimum Wind Speed

The performance of the proposed method has also been established with wind-speed dynamics in the presence of NL load (25% NL + 75% linear load) for an SCR of 2.74, as illustrated in Fig 3.9. This case study aims to address PQ issues associated with the wind-speed (W_{speed}) variations. The wind speed has been decreased from 15 m/s to 7.5 m/s at time t=3.5-second. No changes are observed in the grid voltage (v_{ga}), NL load current (i_{la}), unit templates (ut_a), and error ($error_{pa}$) signals. The DC-link voltage of wind (v_{dcw}) and DSTATCOM (v_{dcd}) are maintained at reference value excepting a few fluctuations due to controlled action. However, generated power (P_w), grid current (i_{ga}) and reactive power (Q_d) of DSTATCOM are decreases with the wind rotor speed (Wr_w). During this process the grid currents remains sinusoidal and balanced. The grid current harmonic (1.18%) and grid voltage harmonics (4.18%) are well maintained to meet the PQ standards.

3.5.4 Case-4: Effect of Variation in Grid SCR

The proposed method has been tested for unbalanced studies by varying the SCR from 2.74 to 7 with different compositions of loads. The harmonics analysis of simulation studies are present in Table 3.4. The DSTATCOM injects reactive power (Q_d) at the PCC to maintain the active power of the wind (P_w), grid voltage (V_g), power factor (PF_g). The voltage (V_{gTHD}) and current (i_{gTHD}) harmonics are limited to the acceptable values as per the PQ standards. The variations in the SCR values from 2.74 to 7 illustrated that slight changes are observed in the second and third decimal of harmonics values. Thus changes in SCR of the ac grid has a negligible effect on the performance of the proposed method.

This can also be verified through the stability analysis of the system is carried out for various strengths of the grid using the Bode stability plot. The transfer function $T_g(s)$ for various short circuit ratios of the grid using grid impedance and controller input gains is written as:

$$T_g(s) = T_p(s) \times T_c(s) = \left[\frac{1}{sZ_g} \times (k_p + \frac{k_i}{s})\right] \tag{3.31}$$

T_p(s); Plant transfer function, T_c(s); PI transfer function and Z_g: grid impedance of different SCRs. Fig. 3.10 shows that the stability of the system is degraded with a grid SCR of 1 due to large

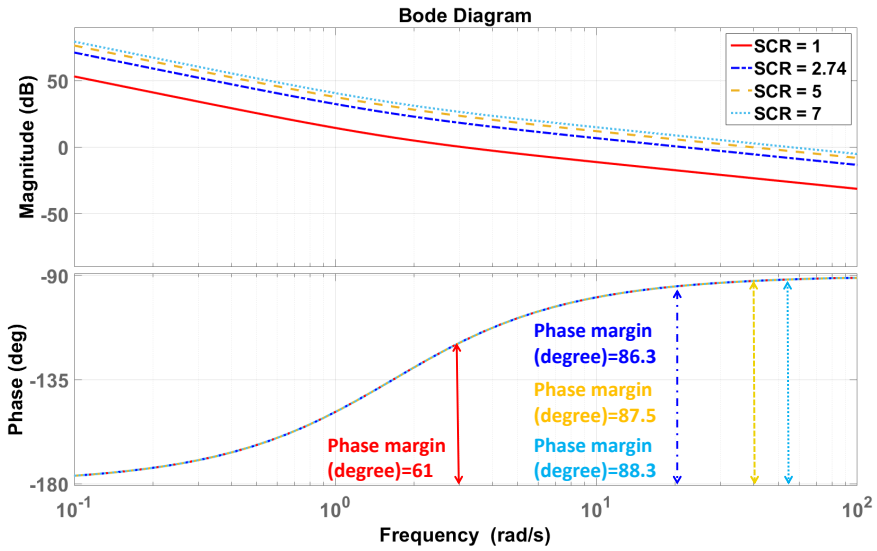

Figure 3.10: Bode stability plot for various grid SCR using grid impedance and controller inputs.

Table 3.4: Performance under variations in grid SCR (Simulation).

Penetration	Loads (→)	load-1			Load-2		
levels (↓)	SCR (→)	2.74	5	7	2.74	5	7
		Simulation analysis					
10%	V_{gTHD}	2.175	2.151	2.140	4.457	4.433	4.422
	i_{gTHD}	0.627	0.603	0.592	1.088	1.01	0.935
	PF_g	1	1	1	0.99	0.99	0.99
	P_w (MW)	1.5	1.5	1.5	1.5	1.5	1.5
	Q_d (MVAr)	0.410	0.401	0.392	0.504	0.495	0.486
	V_g (Volt)	418	417	416	418.5	417.5	418
18%	V_{gTHD}	2.289	2.251	2.230	5.549	5.501	5.421
	i_{gTHD}	0.685	0.661	0.620	1.148	1.124	1.103
	PF_g	1	1	1	0.99	0.99	0.99
	P_w (MW)	3	3	3	3	3	3
	Q_d (MVAr)	0.495	0.481	0.473	0.608	0.594	0.585
	V_g (Volt)	419.09	418.02	416	419.98	418.05	416
25%	V_{gTHD}	2.55	2.50	2.47	7.57	7.51	7.47
	i_{gTHD}	0.71	0.70	0.68	1.41	1.39	1.34
	PF_g	0.99	0.99	0.99	0.99	0.99	0.99
	P_w (MW)	4.5	4.5	4.5	4.5	4.5	4.5
	Q_d (MVAr)	0.99	0.945	0.9	1.215	1.17	1.125
	V_g (Volt)	428.37	428.02	426	428.5	426.03	426.01
30%	V_{gTHD}	4.34	4.22	4.27	9.13	8.88	8.84
	i_{gTHD}	1.88	1.80	1.77	3.24	3.11	2.80
	PF_g	0.89	0.89	0.89	0.67	0.67	0.67
	P_w (MW)	5.56	5.56	5.56	5.52	5.52	5.52
	Q_d (MVAr)	1.96	1.87	1.78	2.40	2.31	2.22
	V_g (Volt)	420.2	420.01	419.7	605.7	603	599.2

impedance, and performance is observed as unsatisfactory. The phase margin of grid impedances of SCR-2.74 and SCR-7 are located in the stable region, indicating that the SCR of 2.74 and beyond the system is stable.

3.5.5 Case-5: Synchronization of DFIG with Rural Grid

1. **Transient Analysis:** The transient analysis for soft synchronization of DFIG into the weak grid (SCR=2.74) at 25% WE penetration is presented in Fig. 3.11. The combination of the load is 25% NL load + 75% linear load. The WE source and DSTATCOM are connected at 1-second, illustrating the transition condition. During this condition (1.0 to 1.02-s), the synchronization starts and the grid voltage (v_g), currents (i_g) are visualized out-of-phase with few notches. The time instant is 1.4 to 1.52-s, the system continuously updates, but after 1.5-s, unexpected operational behaviour is observed. These changes occurred due to the WE sources starting injection of rated active power at PCC. These sudden changes generate large fluctuations in the signals. Therefore, reactive power demand increases significantly to maintain the rated active power of the WE, voltage and harmonics at PCC.

   The proposed method actively manages the expected reactive power to sustain the PCC voltage (±10%) and continuously mitigate the PQ disturbances with less time. The updated stage confers that the algorithm adjusts the changes associated with the system and constantly

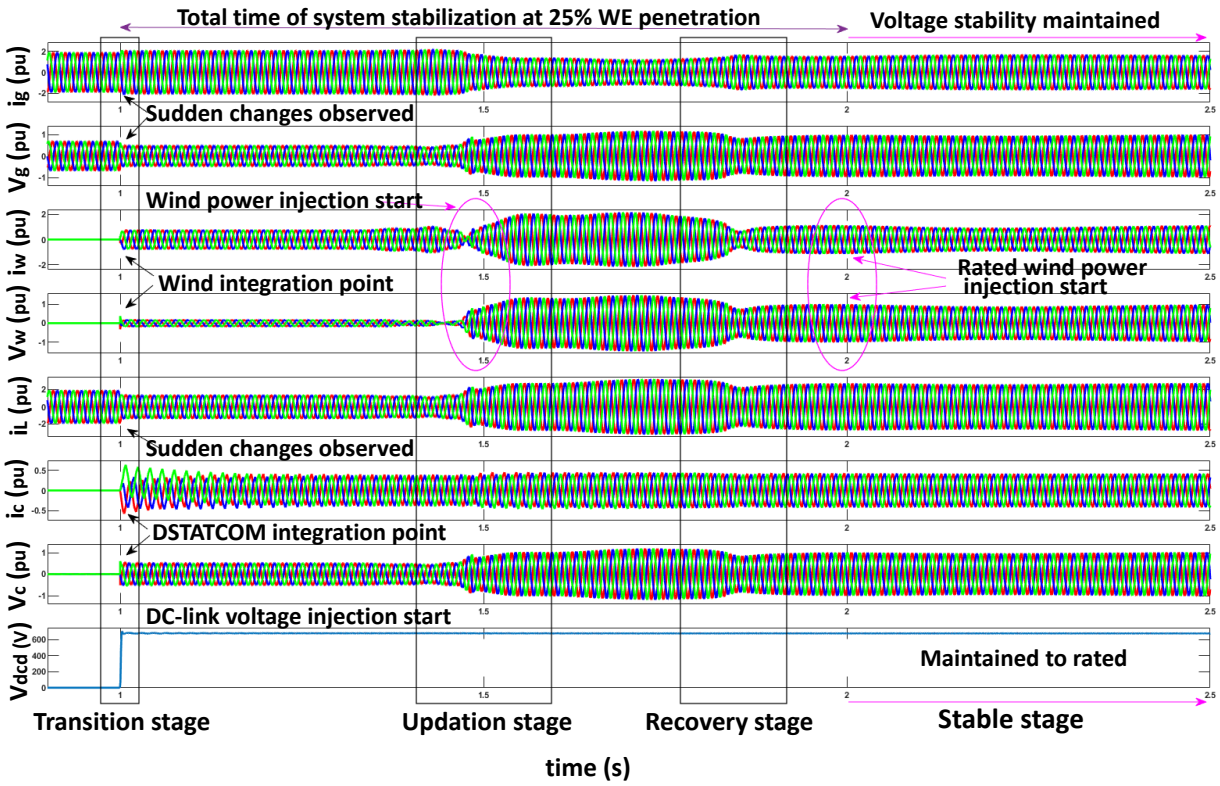

Figure 3.11: Soft synchronization of DFIG with rural grid.

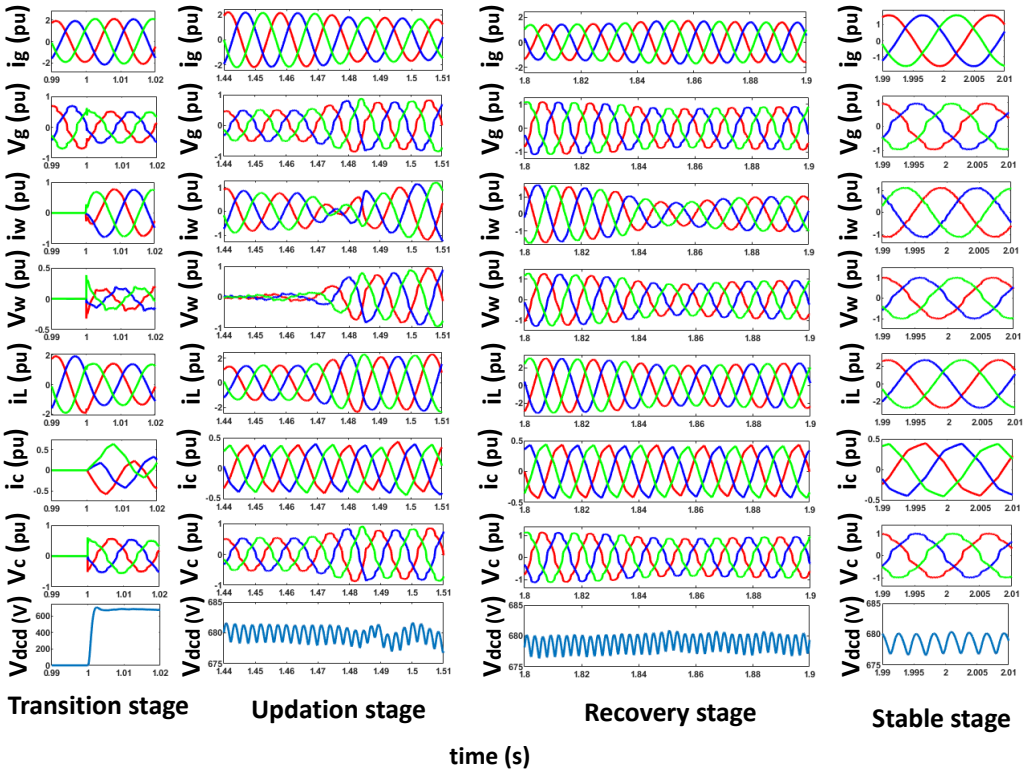

Figure 3.12: Zoomed explanation of Figure 3.11.

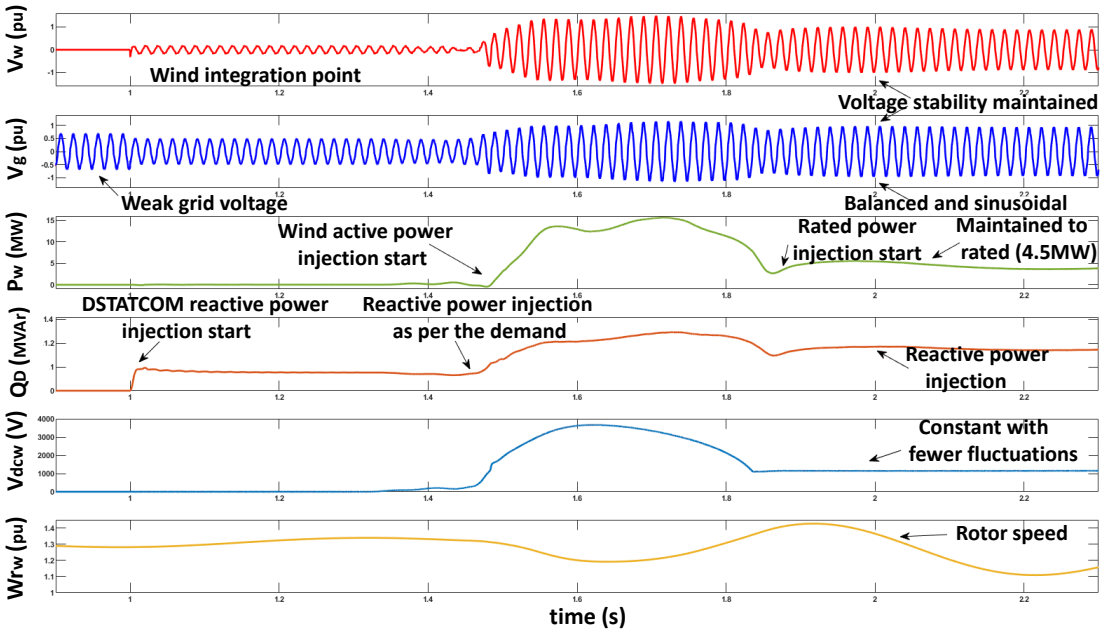

(a)

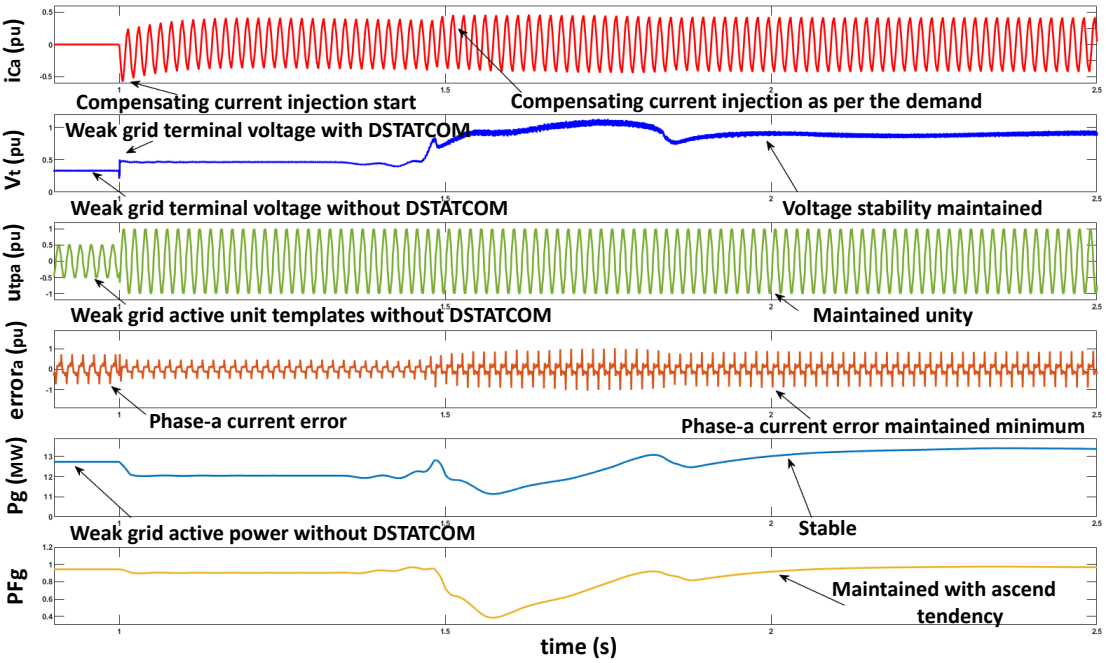

(b)

Figure 3.13: Signals computed using proposed method.

controls the dynamics. The zoomed explanation of both transition and updation stages are depicted in Fig. 3.12.

2. **Steady-State Analysis:** The steady-state analysis considered recovery and stable stages as shown in Fig. 3.11. The instant 1.8 to 1.9-s recovery stage illustrated that all the signals continuously recover and shift at a stable stage with lesser time. The stable stage starts from 1.99-s, and grid voltage and currents are observed sinusoidal and balanced. Therefore, the simulation observations established that <0.9-s is needed for maintaining soft synchronization of DFIG into the grid with SCR of 2.74 and the presence of NL loads. The zoomed waveforms of both recovery and stable stages are presented in Fig. 3.12.

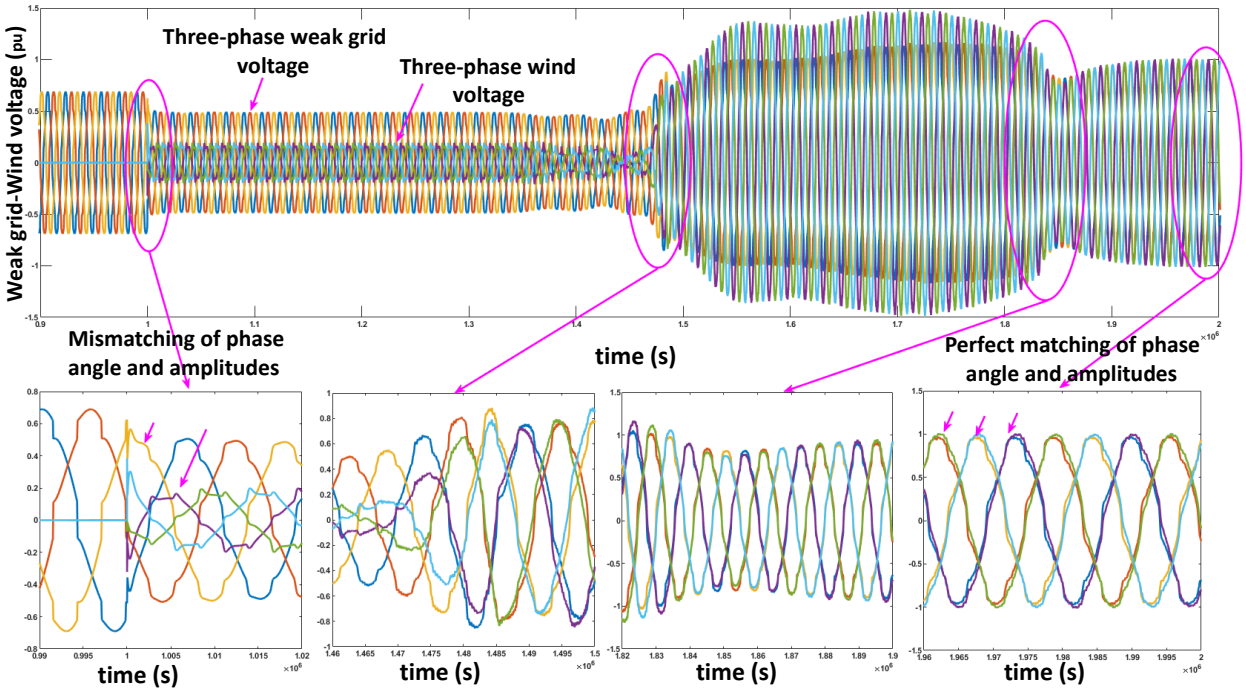

Figure 3.14: Perfect matching of weak grid and wind voltages.

3. **Combined Transient and Steady-State Analysis:** The combined transient and steady-state analysis considered transition, updation, recovery, and stable stages presented in Fig. 3.13. Fig. 3.13 (a) illustrated that the proposed method inject up to 1.5 MVAr reactive power (Q_D) for soft synchronization of DFIG into the weak grid with maintaining rated 4.5 MW active power of the wind (P_w). Thus, it has been found that the proposed control not only maintained reactive power flow, PQ and stability but also reduced the rating of the DSTATCOM by 65%. Moreover, the proposed algorithm does not affect the working of the built-in converter of DFIG. Therefore, built-in converters dc-link voltage is observed at 1150 V, which confers the stable status of the system and applicability of the proposed control.

   The signals computed in the ADALINE-LMS algorithm is as illustrated in Fig. 3.13(b). The perceived results reveal that the DSTATCOM continuously injects the compensating current (i_{ca}) to stabilize the terminal voltage (V_t) under the stability limit (i.e. $\pm 10\%$). The grid active voltage unit template of phase-a (ut_a) is kept at unity during the synchronization. The phase-a current error ($error_a$) is observed negligible. The active grid power (P_g) is found stable, and the grid power factor (PF_g) is visualized with ascending tendency.

   Fig. 3.14 depicted the perfect matching of three-phase grid voltage and WE voltage at PCC. It has been seen that at 1-s, WE source integrated into the grid. During this time, all the phase amplitudes and phase angles are mismatched due to the effective compensation method at 1.99-s achieving perfect synchronization within the voltage stability range as per the standard IEEE-1547.

   The observed weak grid, transient (transition) and steady-state (stable) stages voltage and current harmonics are 13.9%, 14.71%, 7.81% and 7.15%, 4.53%, 1.43%, respectively.

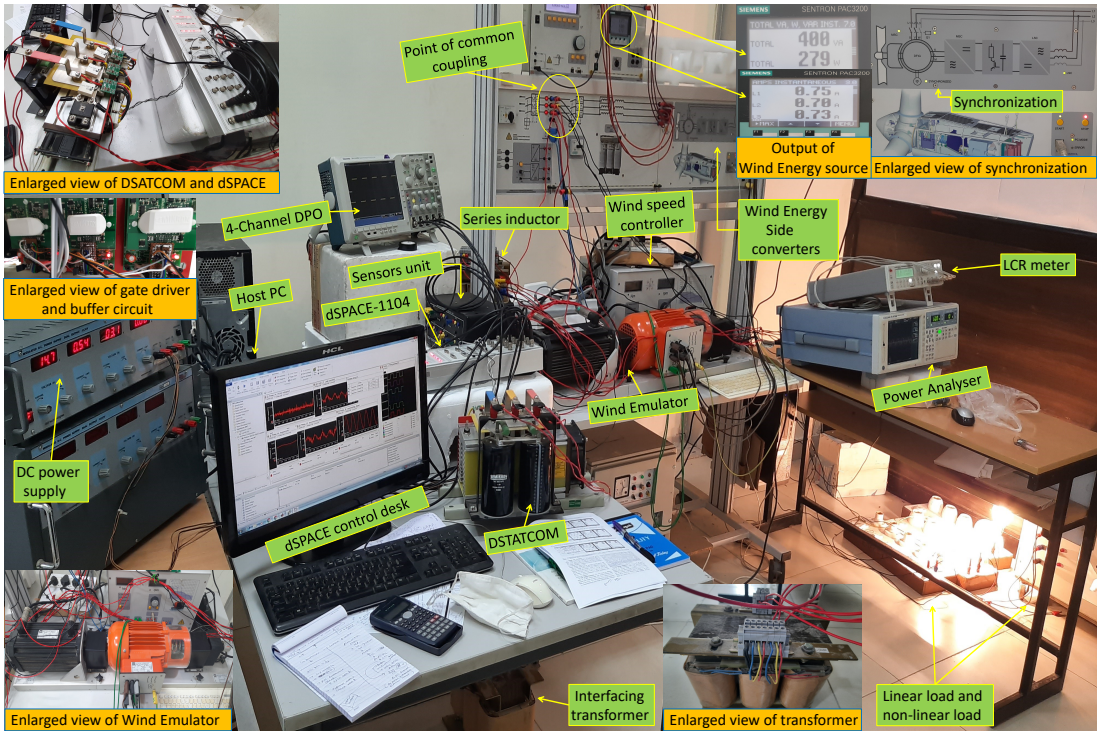

Figure 3.15: Laboratory-based experimental prototype.

3.6 EXPERIMENTAL RESULTS AND DISCUSSIONS

The experimental prototype developed in the laboratory is depicted in Fig 3.15. The voltage and current signals are sensed with hall-effect-based sensors (TI-TMCS1100). These sensed signals are pre-processed by a signal conditioning circuit and converted to digital signals by an ADC interface of the dSPACE-1104 controller. The switching signals received from the digital Inputs/Outputs of the dSPACE are amplified using the buffer-circuit (Microchip-TC427). The SEMIKRON makes VSC, and Lucas-Nulle makes the WE emulator are integrated at PCC. The waveforms and PQ are recorded through the oscilloscope (Tektronix DPO4104B) and the power analyzer (YOKOGAWA-WT3000), respectively.

3.6.1 Case-1: Enhancement of WE Penetration Levels

The penetration levels are enhanced from 10% to 30% into the grid of SCR 2.74 with 100% linear load. Figure 3.16 presents the 25 % WE penetration level with its voltage. It can be found that the power quality of the system in terms of voltage is maintained within the stability range (*i.e.* $\pm 10\%$) up to 30% WE penetration level. However, up to 25%, the active power of WE sources is tracked with more than 99% accuracy, and beyond 25%, the wind power tracking accuracy is deteriorated due to PQ issues. The simulation results are shown in Table 3.5. It is found that increments in the penetration level up to 30% harmonic levels also increase in the system. These harmonic levels are well maintained under the international PQ standards. The power factor, the magnitude of voltage and harmonic levels of voltage and current of the grid are observed to meet PQ standards with increments in the penetration level. It has also been observed that the presence of non-linear load also deteriorates the PQ and limit the wind energy penetration levels.

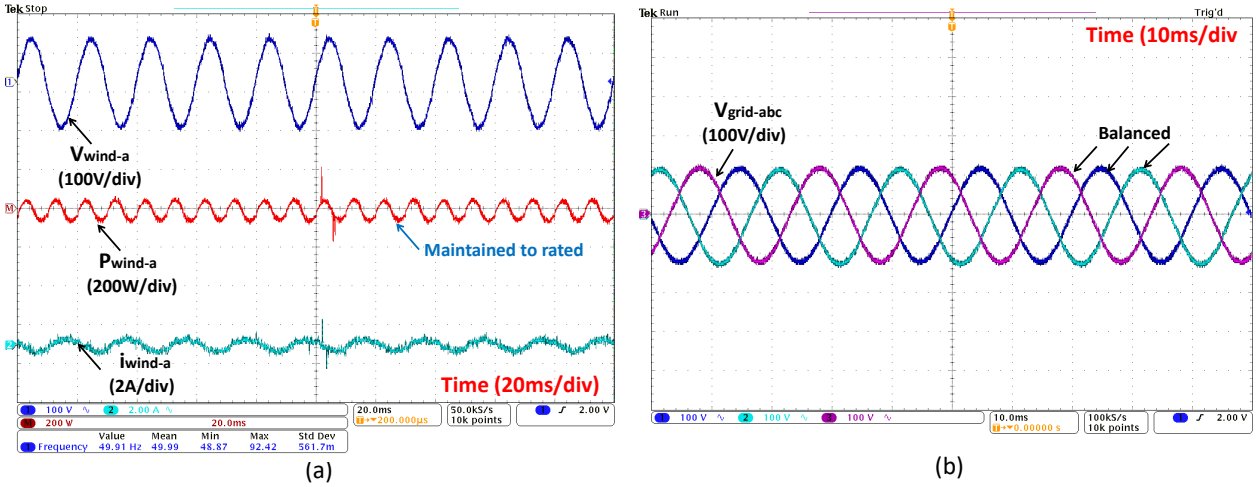

Figure 3.16: WE penetration level with 100% linear load (a) Active power, (b) Grid voltage.

Table 3.5: Enhancement of WE penetration levels (Experimental).

Penetration levels (↓)	Loads (→)	Load-1		
	SCR (→)	2.74	5	7
	Experimental analysis			
10%	V_{gTHD}	2.69	2.52	2.47
	i_{gTHD}	0.987	0.912	0.87
	PF_g	0.99	0.99	1
	P_w (kW)	0.279	0.279	0.279
	Q_d (kVAr)	0.058	0.0573	0.057
	V_g (Volt)	418.27	417.4	417.4
18%	V_{gTHD}	2.92	2.87	2.80
	i_{gTHD}	1.10	1.07	1.01
	PF_g	0.99	0.99	0.99
	P_w (kW)	0.279	0.279	0.279
	Q_d (kVAr)	0.0729	0.072	0.072
	V_g (Volt)	420.87	420.87	420.5
25%	V_{gTHD}	3.07	3.0	2.94
	i_{gTHD}	1.29	1.21	1.17
	PF_g	0.99	0.99	0.99
	P_w (kW)	0.279	0.279	0.279
	Q_d (kVAr)	0.101	0.099	0.096
	V_g (Volt)	430.04	430.04	429.2
30%	V_{gTHD}	5.38	5.01	4.93
	i_{gTHD}	2.96	2.73	2.6
	PF_g	0.84	0.84	0.84
	P_w (kW)	0.271	0.271	0.271
	Q_d (kVAr)	0.21	0.199	0.191
	V_g (Volt)	432.03	431.3	431.1

3.6.2 Case-2: Performance with NL Load at Rated Wind Speed

The WE source is integrated with a grid of SCR of 2.74 in the presence of 25% NL load + 75% linear load. Fig 3.17 (a) demonstrates the injection of compensating currents (i_{C-a}) to

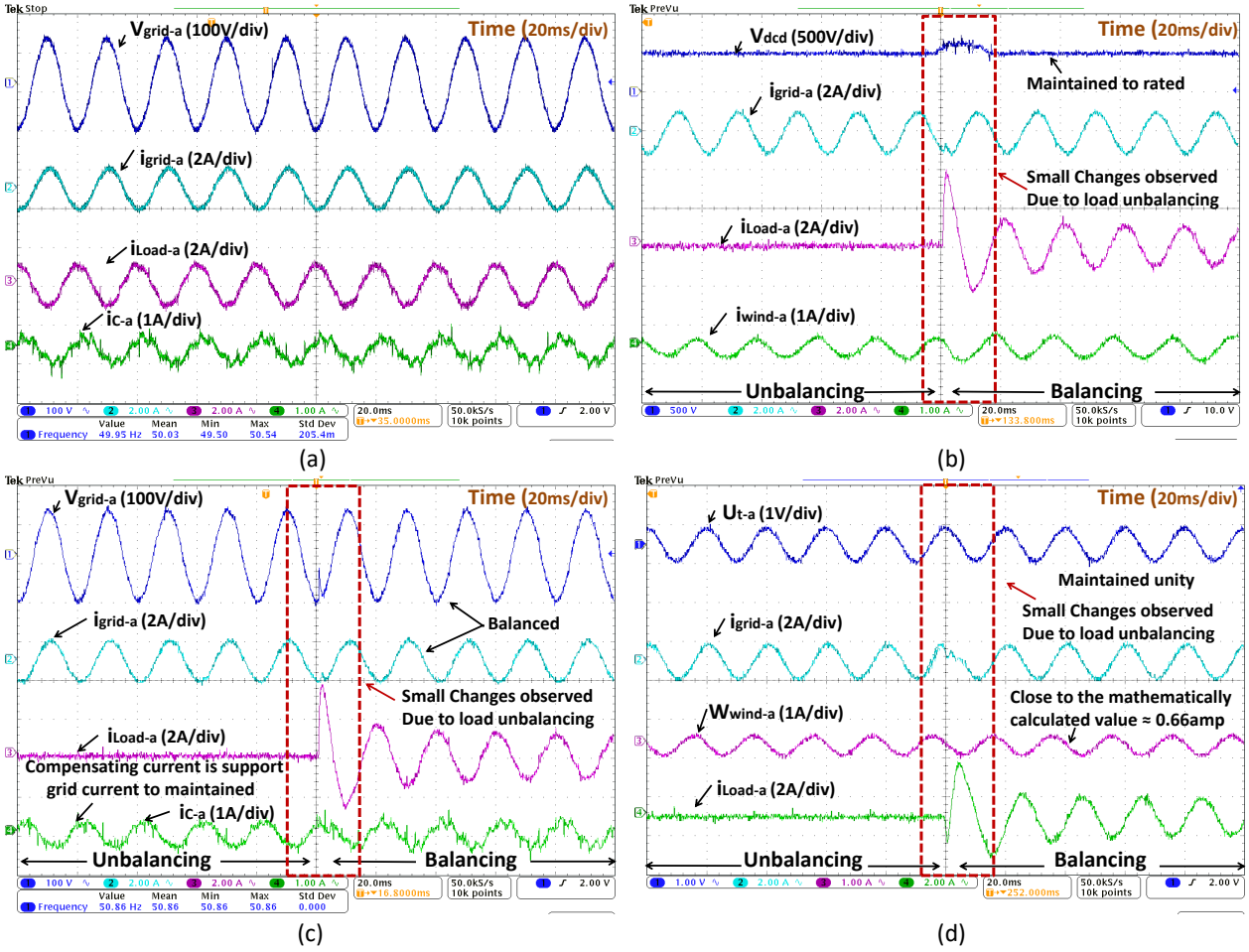

Figure 3.17: Performance of proposed method at rated wind speed. (a) With balanced NL load, and (b),(c),(d) With unbalanced NL load.

maintain grid voltage (V_{grid-a}) and to compensate the grid currents (i_{grid-a}).

The DC-link voltage (v_{dcd}) of the DSTATCOM is maintained at its reference value. The grid current and wind current (i_{wind-a}) remains balanced during the emulated load unbalancing, as illustrated in Fig 3.17 (b). Fig 3.17 (c) illustrates the compensating current being injected to maintain grid voltage and mitigate the unbalance. The steady-state error in the amplitudes of grid current is found to be 0.017 A. During the unbalance, the compensating current is observed non-sinusoidal due to the harmonics present in the wind current.

Fig 3.17 (d) shows that unit voltage template (u_{t-a}) is kept unity. The calculated, simulated and experimental values of wind feed-forward term (W_{wind}) are found to be approximately 0.66 A. This shows the proposed method's efficacy and applicability at weak grids. The three-phase grid currents and load current signals are presented in Fig 3.18 (a)-(d).

3.6.3 Case-3: Performance with NL Load at Minimum Wind Speed

Similar case studies have been performed with the minimum wind speed (7.2 m/s). The grid signals and wind energy signals are depicted in Fig 3.19 (a)-(d). It can be observed that grid voltage (V_{grid-a}) is maintained within the voltage stability limit. The DC-link voltage (v_{dcd}) of the DSTATCOM is found to be stable at reference value. However, the amplitudes of the grid current (i_{grid-a}) and wind current (i_{wind-a}) signals are found less due to the reduction in the wind speeds.

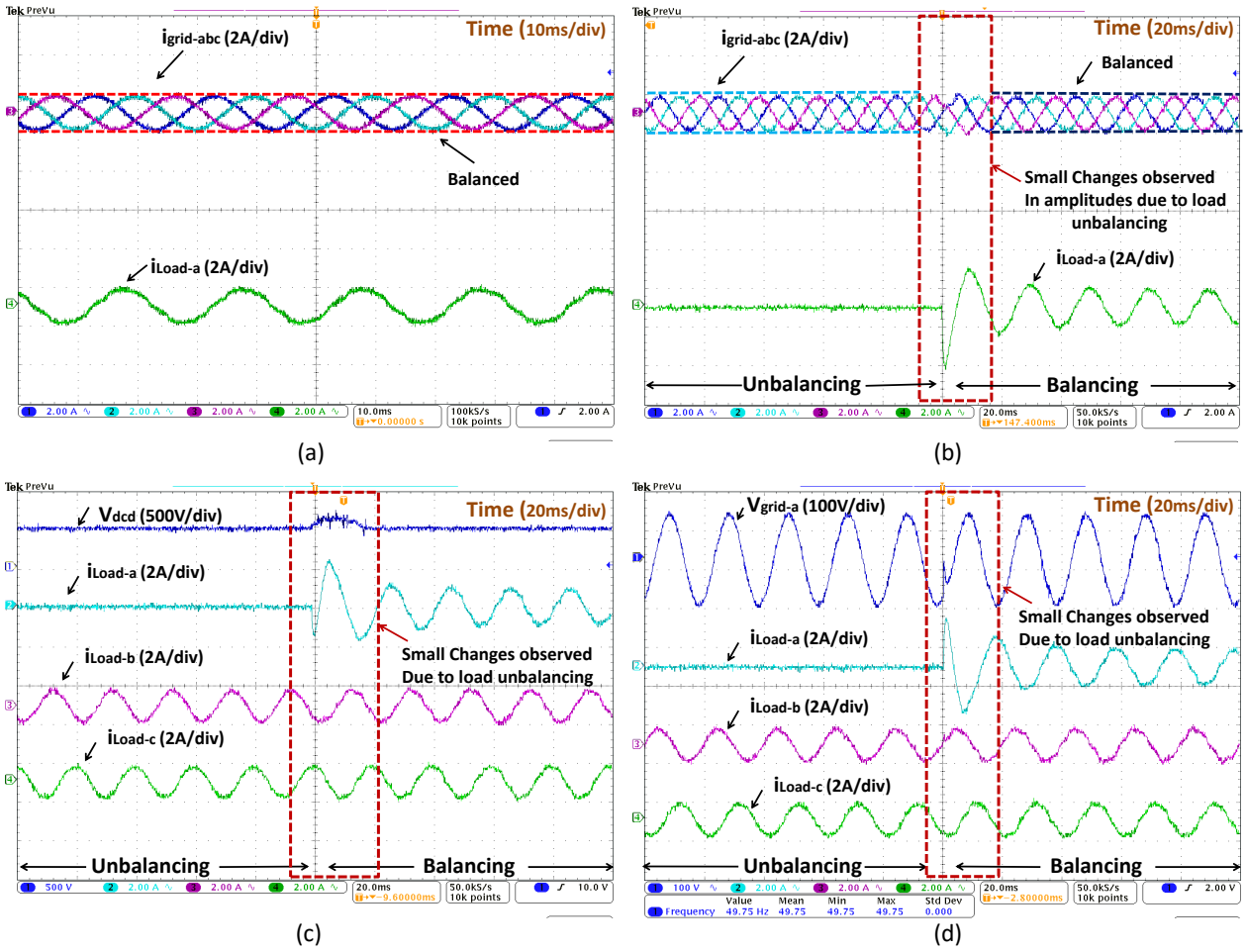

Figure 3.18: Performance of proposed method at rated wind speed. (a) With three-phase balanced NL load, and (b),(c),(d) With unbalanced three-phase NL load.

The harmonic levels of voltage and current are found to be 5.82% and 1.97%, respectively.

3.6.4 Case-4: Effect of Variation in Grid SCR

The proposed method has been tested for unbalanced studies by varying the SCR from 2.74 to 7 with different compositions of loads. The harmonics analysis of experimental studies is present in Table 3.6. The DSTATCOM injects reactive power (Q_d) at the PCC to maintain the active power of the wind (P_w), grid voltage (V_g), power factor (PF_g). The voltage (V_{gTHD}) and current (i_{gTHD}) harmonics are limited to the acceptable values as per the PQ standards. The variations in the SCR values from 2.74 to 7 illustrated that slight changes are observed in the second and third decimal of harmonics values. Thus changes in SCR of the ac grid has a negligible effect on the performance of the proposed method.

3.6.5 Case-5: Synchronization of DFIG with Rural Grid

1. **Transient Analysis:** The phase angle, frequency of grid voltage, and WE voltage are mismatched, as illustrated in Fig. 3.20 (a). However, after applying the proposed method, perfect matching of phase angle, amplitude and frequency of weak grid and WE voltage under NL load is shown in Fig. 3.20 (b). Also, the maximum WE emulator active power is visualized 0.279 kW with the capacity of 0.400 kW in Fig. 3.20 (c).

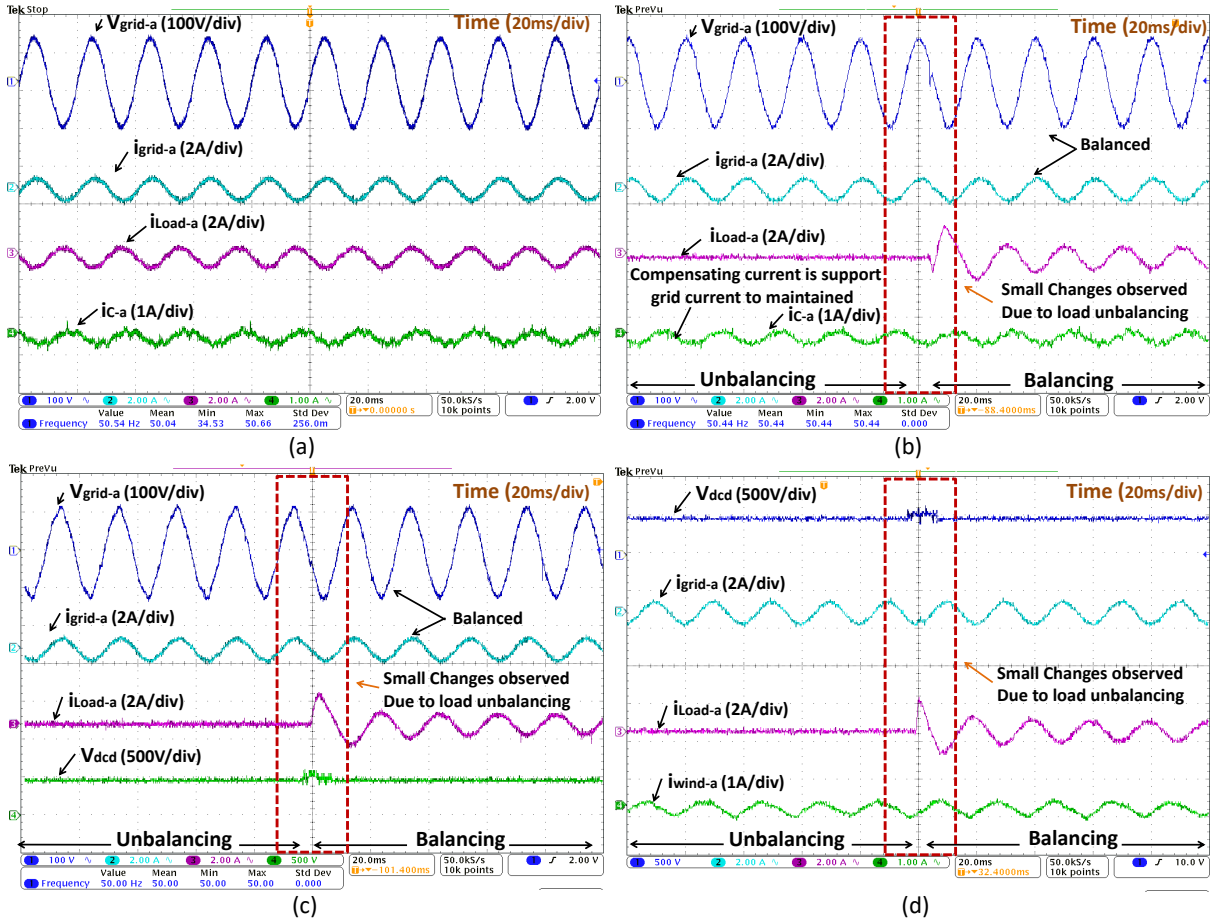

Figure 3.19: Performance of proposed method at minimum wind speed. (a) With balanced NL load, and (b),(c),(d) With unbalanced NL load.

The transient performance of ADALINE-LMS controlled DSTATCOM for the soft grid synchronization is illustrated in Fig. 3.21 (a)-(d). Fig. 3.21 (a) illustrates the harmonics and notches are present in the weak grid voltage (V_{grida}), (V_{gridb}), (V_{gridc}) due to the presence of NL load and DSTATCOM is not injecting required reactive power at PCC. Therefore, DC-link voltage (v_{dcd}) is observed 0 V. The DSTATCOM is connected at PCC to inject demanded reactive power ($Q_{dstatcom}$) up to 0.046 kVAr/phase to maintain the synchronization requirements with high wind penetration level (25%). The distortion in the reactive power waveform of DSTATCOM is observed due to the non-sinusoidal reactive power injected by the compensator to compensate for the non-linear load. However, distortion in the waveform of the active power of WE sources ($P_{wind} = 0.093kW/phase$) is identified after the synchronization due to the residual harmonics. The wind current (i_{winda}) of 0.7 A and wind voltage (V_{winda}) have been visualized with fewer fluctuations at rated active power penetration of WE source. Meanwhile, harmonics are observed in the grid voltage, and terminal voltages are observed before the integration of DSTATCOM presented in Fig. 3.21 (c). After integrating DSTATCOM and WE sources, DC link voltage injection is started and maintains the grid voltage. The unit voltage template (u_{ta}) is found to be unity shows fulfilling the amplitude requirement of soft synchronization. The auxiliary wind feed-forward term (W_{wind}) is maintained at 0.665 A, which is approximately similar to the calculated and simulated value that shows the effectiveness of the proposed adaptive capability of the ADALINE-LMS algorithm.

2. **Steady-State Analysis:** The transient performance of ADALINE-LMS controlled

Table 3.6: Performance under variations in grid SCR (Experimental).

Penetration levels (↓)	Loads (→)	Load-1			Load-2		
	SCR (→)	2.74	5	7	2.74	5	7
Experimental analysis							
10%	V_{gTHD}	2.69	2.52	2.47	4.937	4.87	4.74
	i_{gTHD}	0.987	0.912	0.87	1.392	1.31	1.24
	PF_g	0.99	0.99	1	0.99	0.99	1
	P_w (kW)	0.279	0.279	0.279	0.279	0.279	0.279
	Q_d (kVAr)	0.058	0.0573	0.057	0.0766	0.0751	0.0750
	V_g (Volt)	418.27	417.4	417.4	418.27	417.4	417.4
18%	V_{gTHD}	2.92	2.87	2.80	5.35	5.21	5.17
	i_{gTHD}	1.10	1.07	1.01	1.87	1.81	1.73
	PF_g	0.99	0.99	0.99	0.99	0.99	0.99
	P_w (kW)	0.279	0.279	0.279	0.279	0.279	0.279
	Q_d (kVAr)	0.0729	0.072	0.072	0.09156	0.090	0.090
	V_g (Volt)	420.87	420.87	420.5	420.9	420.9	420.4
25%	V_{gTHD}	3.07	3.0	2.94	7.723	7.651	7.58
	i_{gTHD}	1.29	1.21	1.17	2.035	1.972	1.831
	PF_g	0.99	0.99	0.99	0.99	0.99	0.99
	P_w (kW)	0.279	0.279	0.279	0.279	0.279	0.279
	Q_d (kVAr)	0.101	0.099	0.096	0.1186	0.117	0.116
	V_g (Volt)	430.04	430.04	429.2	430.05	430.05	429.53
30%	V_{gTHD}	5.38	5.01	4.93	9.87	9.73	9.47
	i_{gTHD}	2.96	2.73	2.6	4.17	3.93	3.73
	PF_g	0.84	0.84	0.84	0.67	0.67	0.67
	P_w (kW)	0.271	0.271	0.271	0.271	0.271	0.271
	Q_d (kVAr)	0.21	0.199	0.191	0.24	0.234	0.231
	V_g (Volt)	432.03	431.3	431.1	610.6	610.7	608.2

DSTATCOM for the soft grid synchronization is illustrated in Fig. 3.21 (e)-(f). Three-phase grid voltage ($V_{grid-abc}$) is found to be sinusoidal and balanced.The DSTATCOM DC-link voltage (v_{dcd}) is found stable (500 V) and maintained at a set reference value shown in Fig. 3.21 (e). It can also be visualized that synchronization is achieved with the grid frequency (F_{grid}) of 49.96 Hz.

It has been found from Fig. 3.21 (f) that compensating current (i_{ca}) of 0.9 A is added by the DSTATCOM to maintain weak grid voltage (V_{grida}) within the stability limit and compensate the non-linearity of the loads. The grid current (i_{grida}) of 2 A and voltage are continuously balanced and remains sinusoidal with the non-linear load (i_{Loada}) of 2 A.

3. **Combined Transient and Steady-State Analysis:** Fig. 3.21 (b)-(c) depicted that the reactive power (0.046 kVAr/phase) is added by the DSTATCOM to maintain the weak grid voltage for the soft grid synchronization and allow the WE source to inject rated power (0.093kW/phase) at PCC. However, the size of DSTATCOM is considered 0.400 kVAr equivalents to the WE source, without a controller. It can be found that DSTATCOM size is reduced by 65% for soft synchronization of DFIG in the weak grid.

   The active grid power delivered at PCC is 0.448 kW/phase (i.e. 1.34 kW). The active wind power delivered at PCC is 0.093 kW/phase (i.e. 0.279 kW). The total generated power (i.e. 1.34 kW + 0.279 kW = 1.619 kW) supply to the 1.6 kW load illustrated in Fig. 3.22.

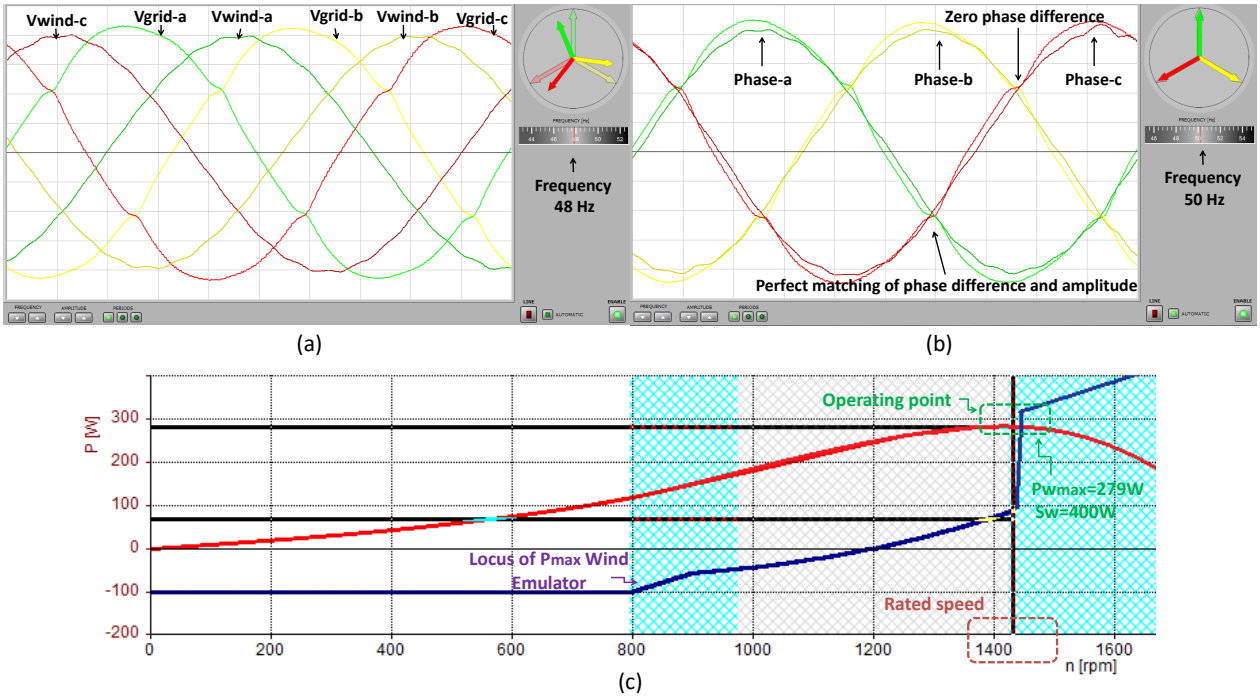

Figure 3.20: (a) Unsynchronized wind and grid voltages and (b) Synchronized wind and grid voltages. (c) Maximum rated active power of the wind energy emulator.

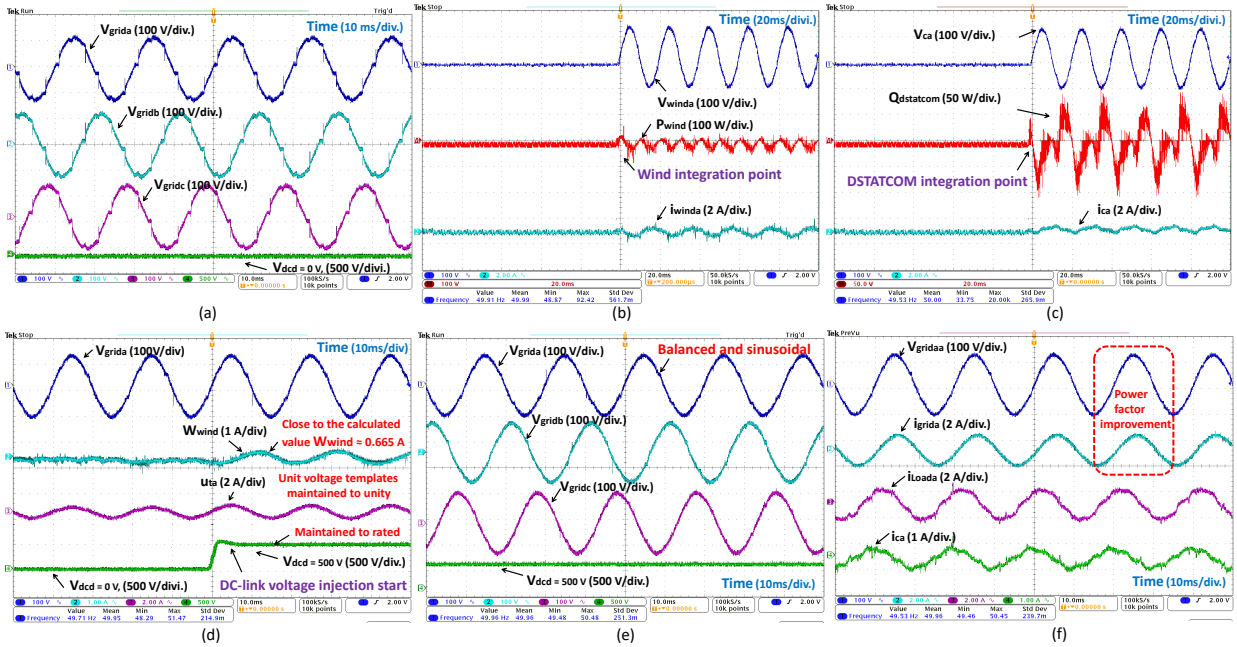

Figure 3.21: (a) Weak grid signals without DSTATCOM. Transient conditions of (b) Wind, (c) DSTATCOM and (d) Intermediate signals. Steady-state conditions of (e) Grid and (f) DSTATCOM signals.

The observed weak grid, transient (transition) and steady-state (stable) stages voltage and current harmonics are 14.7%, 16.79%, 7.923% and 9.5%, 5.13%, 1.67%, respectively.

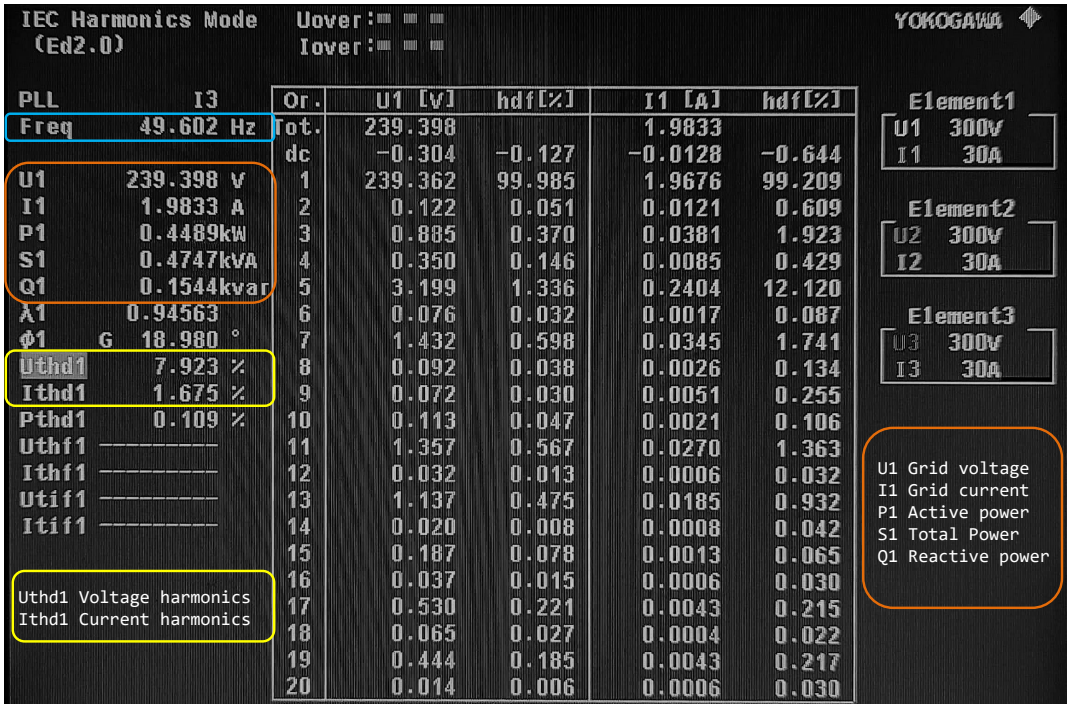

Figure 3.22: Harmonics and power flow analysis under synchronization condition.

Table 3.7: Performance under synchronization of DFIG with rural grid.

Loading condition	Synchronization stages	MATLAB Simulation Results (MSR)			Experimental Results (HR)		
		THDVg (%)	THDig (%)	PFg	THDVg (%)	THDig (%)	PFg
Load-1	Weak grid	13.9	7.15	>0.7	14.7	9.5	>0.7
	Transition	14.71	4.53	>0.7	16.79	5.13	>0.7
	Stable	7.81	1.43	0.96	7.923	1.67	0.94
Load-2	Weak grid	15.7	9.77				
	Transition	19.17	7.03				
	Stable	11.68	2.58	0.87			
Load-3	Weak grid	19.14	13.31				
	Transition	23.54	12.33				
	Stable	13.86	6.01	0.86			
Load-4	Weak grid	23.57	17.64				
	Transition	29.88	28.65				
	Stable	16.53	9.92	0.59			

4. **Effect of high percentage NL load:** The algorithm's performance has been tested for different compositions loads by varying the percentage of NL loads (i.e. Load-1=25%, Load-2=50%, Load-3=75% and Load-4=100% NL loads). The harmonics analysis of both simulation and Experimental results are presented in Table 3.7. The results reveal that there is a trade-off between the soft synchronization of DFIG with a high wind penetration level (25%) and the NL loads (beyond 25%). Therefore, such a situation is more challenging and strongly requires more focus.

3.7 HARMONICS AND POWER FLOW ANALYSIS

The harmonics and power flow analysis of the system without DSTATCOM are illustrated in Figure 3.23 (a). The observed voltage and current harmonic levels are 14.978% and 10.743%, respectively. The active and reactive power are visualized at the PCC are 0.4429 kW/phase and -0.0197 kVAr/phase, respectively. The grid voltage is found to be 201.24 V. These results are not found satisfactory as per the PQ standards. Figure 3.23 (b) illustrated the harmonics and power analysis with DSTATCOM. The observed voltage and current harmonic levels are 7.723% and 2.035%, respectively and lie within the unit of PQ standards. The active and reactive power

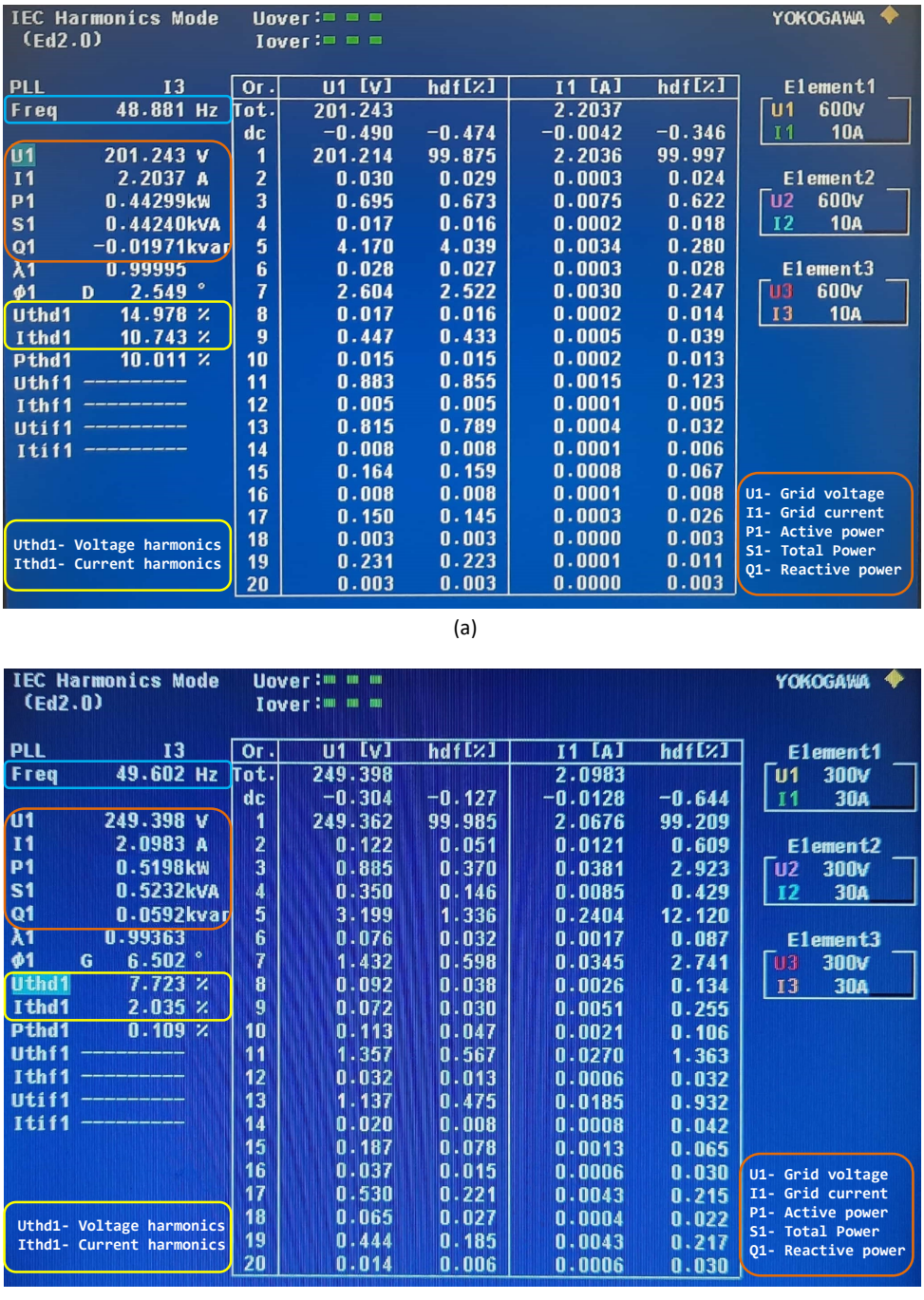

(a)

(b)

Figure 3.23: Harmonics and power flow analysis (a) Without DSTATCOM, (b) With DSTATCOM.

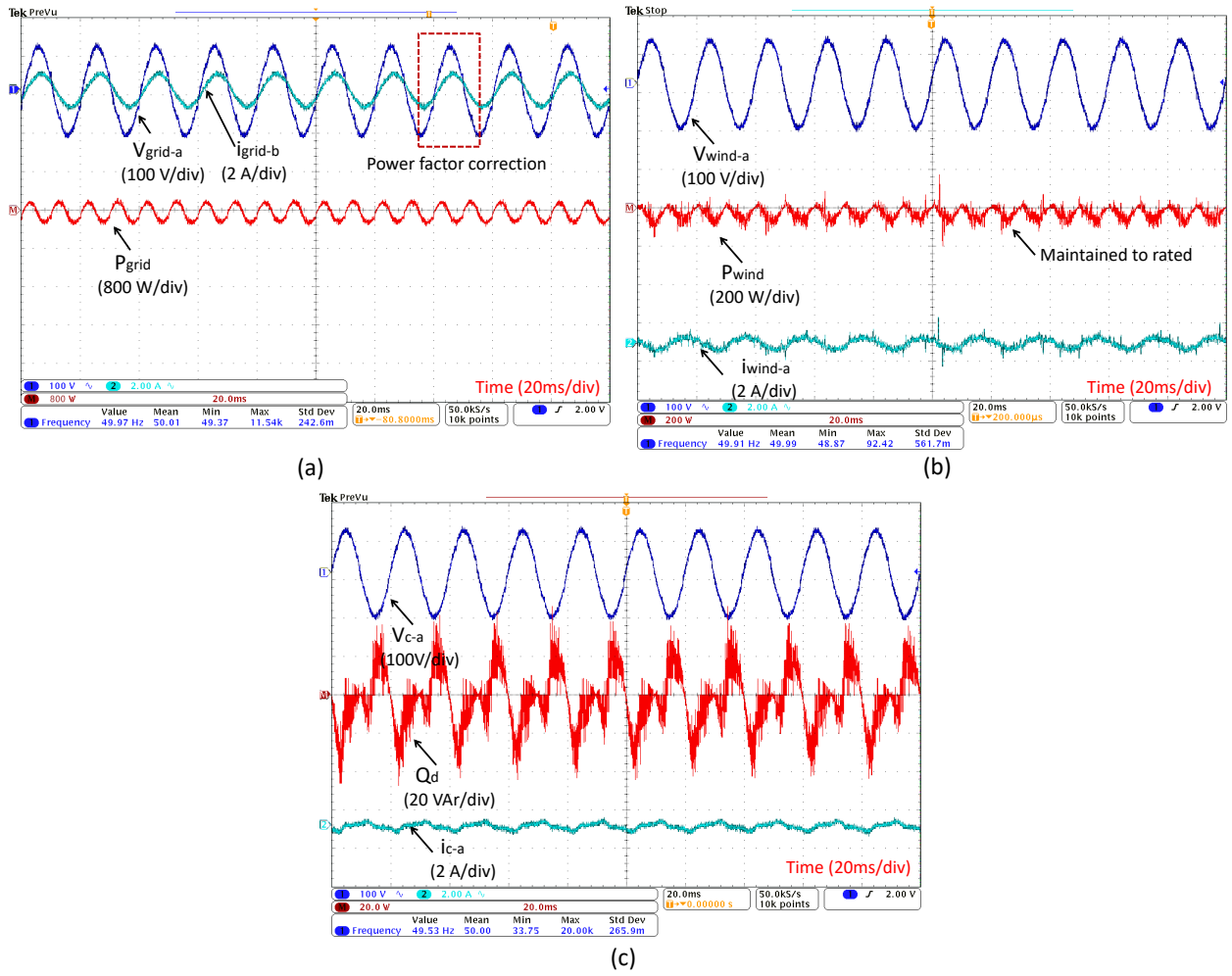

Figure 3.24: Per-phase power analysis (a) Grid, (b) WE source and (c) DSTATCOM.

visualized at the PCC are 0.5198 kW/phase and 0.5198 kW/phase, respectively. The grid's voltage is found to be 249.39 V. These results show that the ADALINE-LMS controlled DSTATCOM injected the required (0.03953 kVAr/phase) reactive power at the PCC to maintain the grid voltage and harmonic levels. Figure 3.24 (a) (b) shows the power analysis of the grid and wind power, which shows that the grid is delivered the 0.4268 kW/phase power (i.e. 1.28 kW) at the PCC along with the 0.093 kW/phase wind power (i.e. 0.279 kW) with the capacity of 0.5232 kW/phase (i.e. 1.57 kW) to supply 0.533 kW/phase (i.e. 1.6 kW) loads. Figure 3.24 (c) illustrated the DSTATCOM is injected up to 0.03956 kVAr/phase reactive power (i.e. 0.1185 kVAr). However, 0.01 kW/phase (i.e. 0.03 kW) of power loss is detected at the PCC. The size of DSTATCOM has been considered 0.400 kVAr, without a controller. However, after implementing the proposed adaptive control algorithm, the optimized reactive power injected by DSTATCOM during 25% WE penetration is approximately 0.1185 kVAr. This result shows the size of DSTATCOM is reduced by 70% due to effective control actions of the adaptive control algorithm.

3.8 COMPARATIVE ANALYSIS

The same simulation test has been carried out using Synchronous Reference Frame Theory (SRFT) and proposed ADALINE-LMS control algorithms for an SCR of 2.74 with 25% WE penetration. It can be seen from Fig. 3.25 that the fluctuations in dc-bus voltage of DSTATCOM

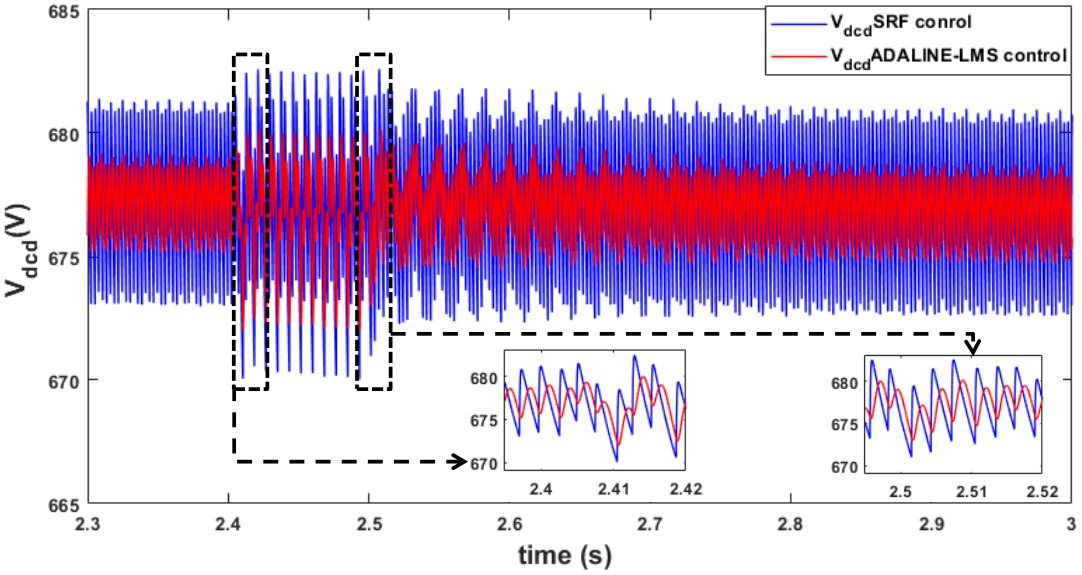

Figure 3.25: DC-link voltage based comparison analysis.

Table 3.8: Comparative analysis.

Attributes	Without control	DSTATCOM with SRFT	DSTATCOM with ADALINE-LMS
Computational burden	-	High	Low
Accuracy of power estimation	3.6 MW	4.2 MW	4.5 MW
Accuracy of voltage tracking	325 V	374 V	427 V
Voltage harmonics Mitigation	13.2%	8.7%	7.57%
Current harmonics Mitigation	9.5%	3.9%	1.41%
Power factor	Fluctuated	0.92	0.99
Stability at SCR < 3	Unstable	Unstable	Stable (phase margin -89.9°)
DC-link voltage of DSTATCOM	-	680 V with high oscillations	680 V
DC-link voltage of built-in converter	1150 V	1150 V	1150 V
Synchronization time	> 3 s	≥ 2 s	< 0.9 s
WE penetration level	20%	22%	25%
Reduction in DSTATCOM size	-	30-50%	70%

were found less with the ADALINE-LMS algorithm compared to the SRF control algorithm. The performance comparison is presented in Table 3.8, which depicts that the ADALINE-LMS control is superior in terms of voltage stability, wind power accuracy, harmonics minimization, oscillations in DC-link voltage, less computational complexity and reduction in DSTATCOM size.

Table 3.9 presents the synchronization time comparison of various methodologies used for WE penetration in adverse operating conditions and the proposed method. It can be perceived from Table 3.9 that the ADALINE-LMS control is superior in terms of providing smooth synchronization of DFIG into the rural grid with 25% WE penetration. The proposed adaptive algorithm also

Table 3.9: Synchronization time comparison under weak system conditions.

Attributes	Improved Stator Voltage Oriented controller [Ghasemi *et al.*, 2020]	Conventional PID [Thakallapelli *et al.*, 2019]	Adaptive PID [Thakallapelli *et al.*, 2019]	Proposed ADALINE-LMS
Synchronization time (s)	≈ 1	≈ 13	$\approx$ 5-11	0.84
Fluctuations in V_{dc}	More	More	More	Fewer

reduced the size of DSTATCOM.

3.9 CONCLUSIONS

In this work, an ADALINE-LMS-based adaptive algorithm is proposed to control DSTATCOM for improving the PQ and thereby enhance the penetration levels in the rural grid in the presence of NL loads under the variations of wind speed. The proposed method has been tested by simulating unbalance in the system and varying the parameters such as SCR, the compositions of linear, NL loads and wind speed. The proposed method has successfully achieved a WE penetration level of 25% into a rural grid of SCR 2.74 in the presence of 25% NL load under wind speed 15 m/s and maintained under 7.5 m/s. The smooth synchronization is also achieved within 0.9 seconds. The accurate signal tracking of the proposed algorithm helps in reactive power planning and thereby optimizes the size of the DSTATCOM. A reduction of 70% in the capacity of the DSTATCOM has been achieved using the proposed algorithm. All simulation and experimental results have achieved the PQ standards laid by EN-50160 and IEEE 519-2014.